Detecting Gravitational Waves

Gabriela González
Louisiana State University

Penn State, June 12 2015

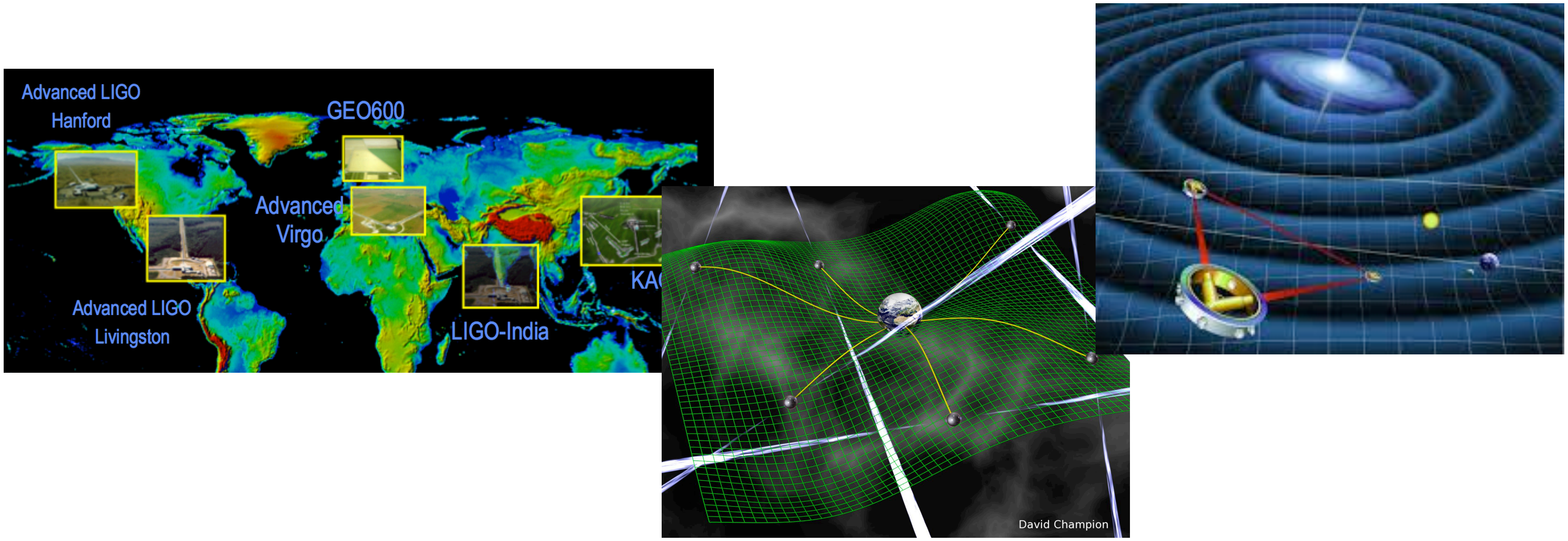

Gravitational waves

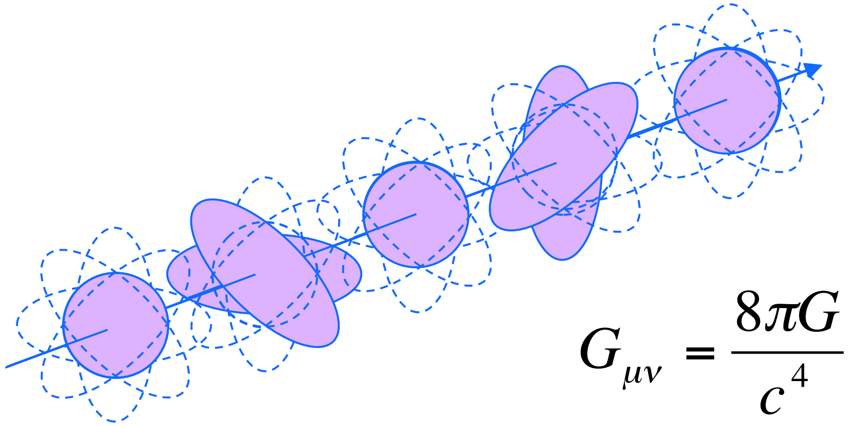

Gravitational waves are quadrupolar distortions of distances between freely falling masses. They are produced by time-varying mass quadrupoles.

$$G_{\mu\nu} = \frac{8\pi G}{c^4} T_{\mu\nu} \; (= 0 \text{ in vacuum})$$

$$g_{\mu\nu} = \eta_{\mu\nu} + h_{\mu\nu} \qquad h = 2\frac{\Delta L}{L}$$

$$h_{\mu\nu} \sim \frac{2G}{c^4 r} \ddot{I}_{\mu\nu}$$

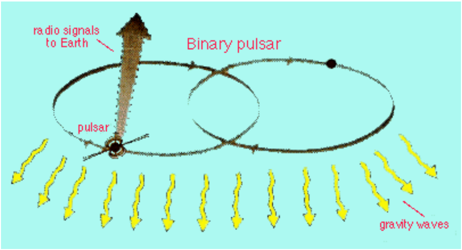

$$h_{\mu\nu} \sim \frac{R_1 R_2}{D r}$$

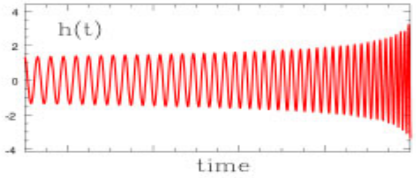

A NS-NS coalescence in the Virgo cluster has $h \sim 10^{-21}$ near Earth:
changes the distance between the Sun and the Earth by ~ one atomic diameter, and changes 1km distance by ~10^{-18} m

GW landscape

Many sources, many frequencies, many detectors, many collaborations

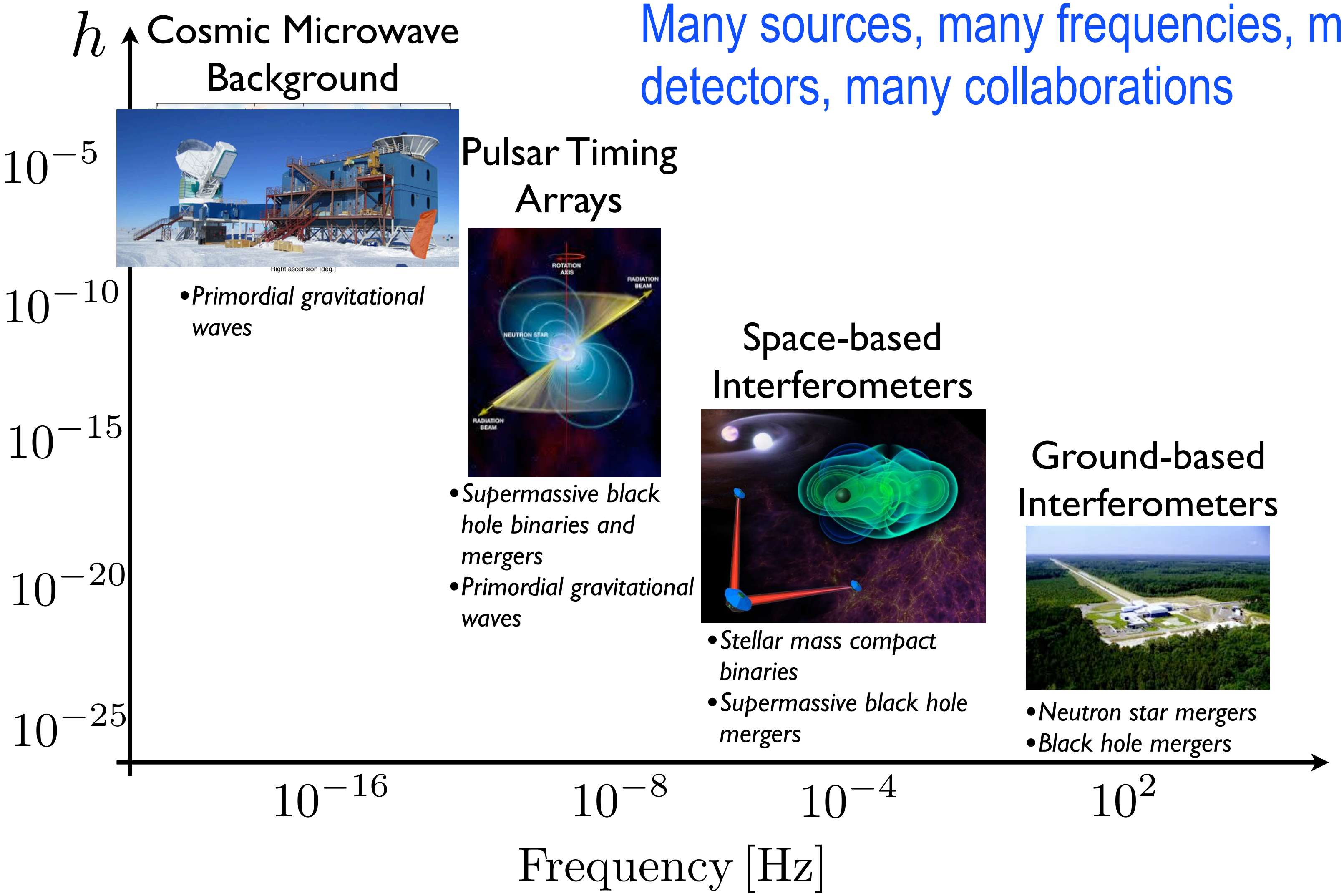

Cosmic Microwave Background

- *Primordial gravitational waves*

Pulsar Timing Arrays

- *Supermassive black hole binaries and mergers*
- *Primordial gravitational waves*

Space-based Interferometers

- *Stellar mass compact binaries*
- *Supermassive black hole mergers*

Ground-based Interferometers

- *Neutron star mergers*
- *Black hole mergers*

Credit: Nanograv/Bicep2

Primordial GWs

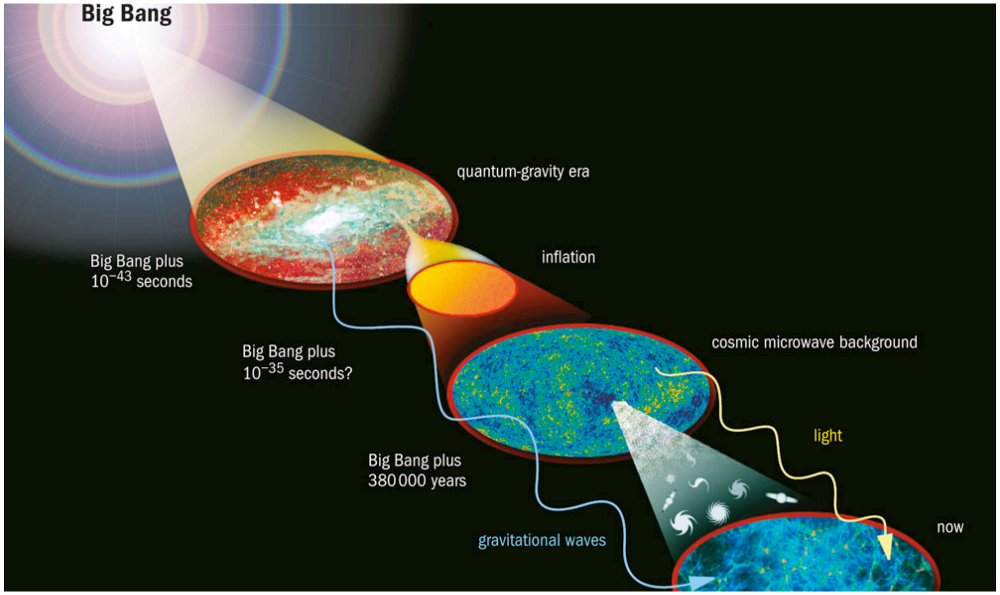

Credit image: NASA

$$\Omega_{\rm gw}(f) \equiv \frac{f}{\rho_c}\frac{d\rho_{\rm gw}}{df}\ .$$

$$S_{\rm gw}(f) = \frac{3H_0^2}{10\pi^2}\, f^{-3}\Omega_{\rm gw}(f)\ .$$

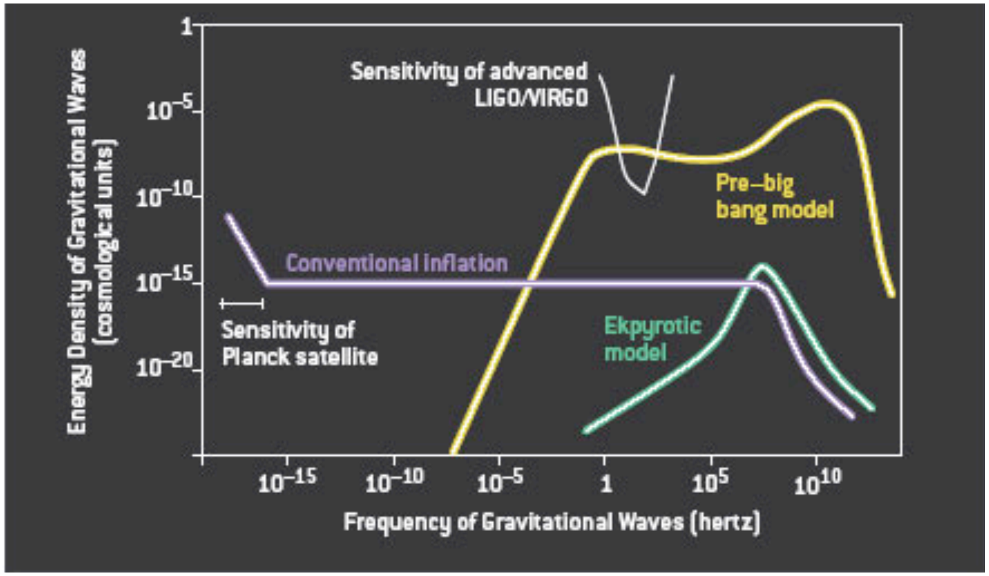

Veneziano, **Scientific American**, 2004, 290, p54-65

Primordial GWs

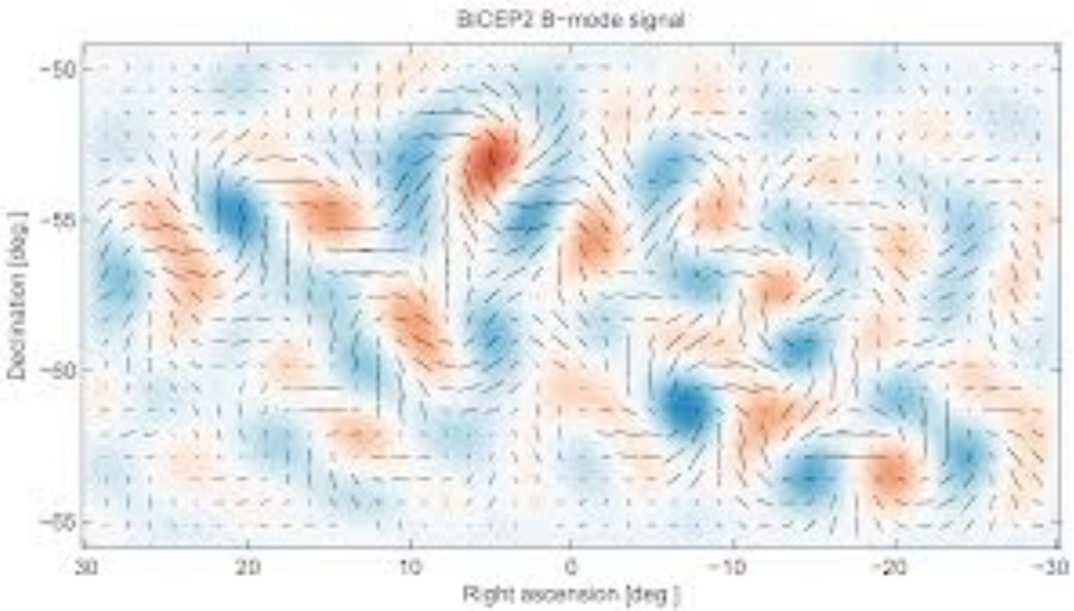

Bicep2, Keck, South Pole

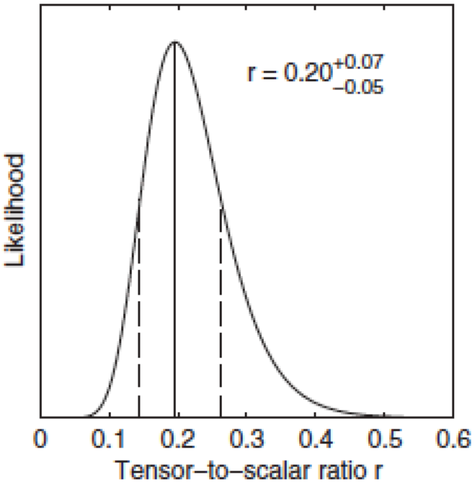

ΛCDM+lensing

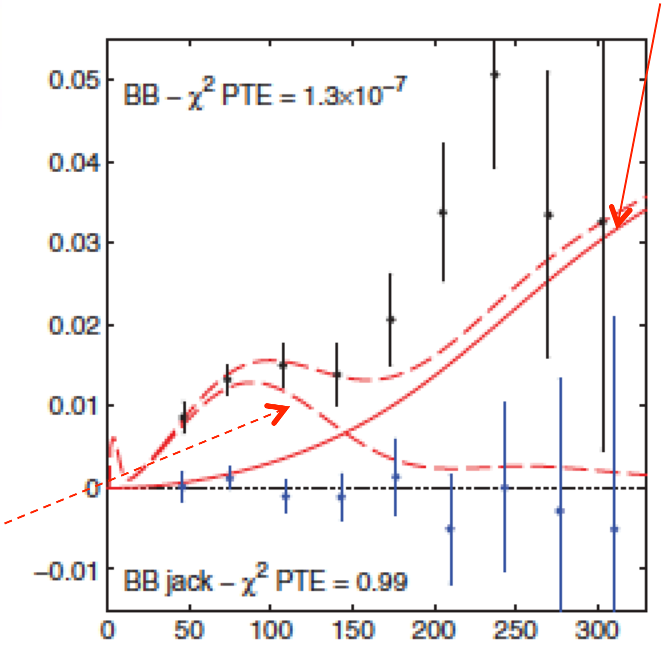

PRL 112, 241101 (2014)

Primordial GWs

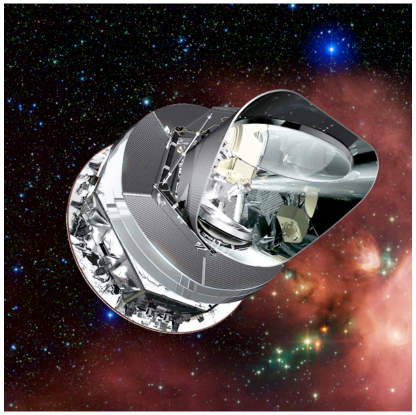

Planck Satellite

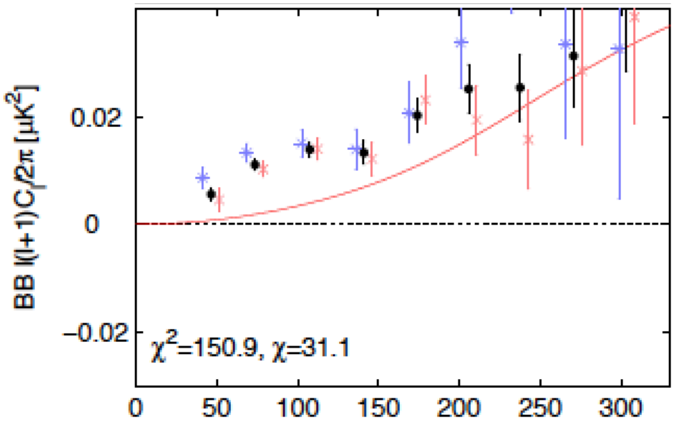

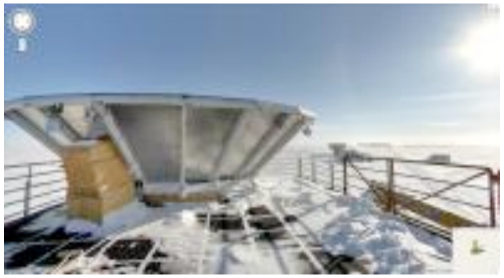

Bicep2, Keck, South Pole

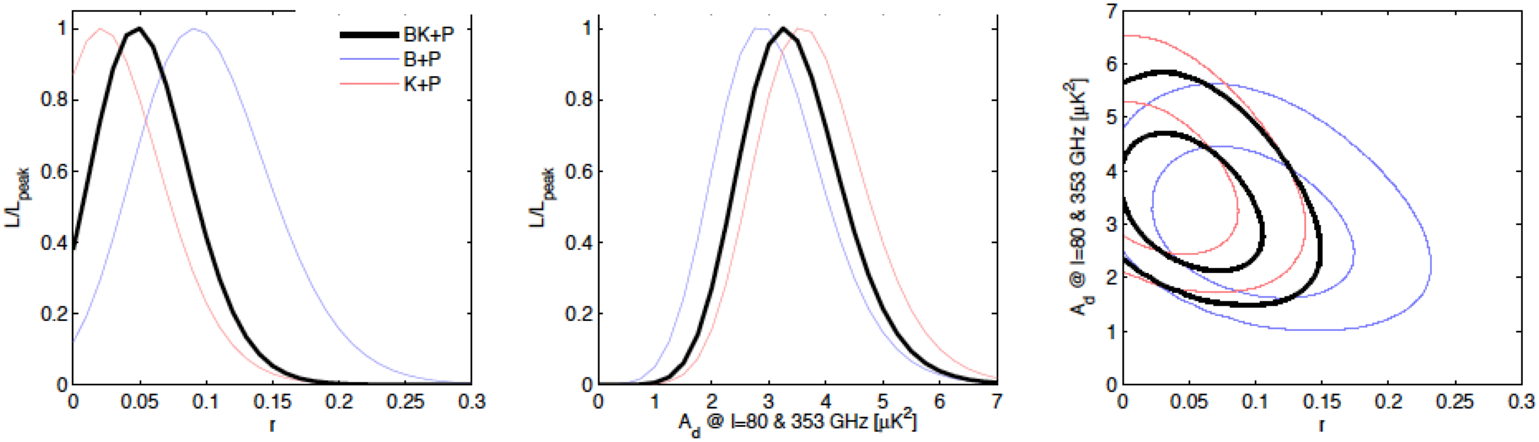

FIG. 6. Likelihood results from a basic lensed-ΛCDM+r+dust model, fitting BB auto- and cross-spectra taken between maps at 150 GHz, 217, and 353 GHz. The 217 and 353 GHz maps come from *Planck*. The primary results (heavy black) use the 150 GHz combined maps from BICEP2/*Keck*. Alternate curves (light blue and red) show how the results vary when the BICEP2 and *Keck Array* only maps are used. In all cases a Gaussian prior is placed on the dust frequency spectrum parameter $\beta_\mathrm{d} = 1.59 \pm 0.11$. In the right panel the two dimensional contours enclose 68% and 95% of the total likelihood.

P. A. R. Ade *et al.* (BICEP2/Keck and Planck Collaborations)
Phys. Rev. Lett. 114, 101301

GW detection with an interferometer

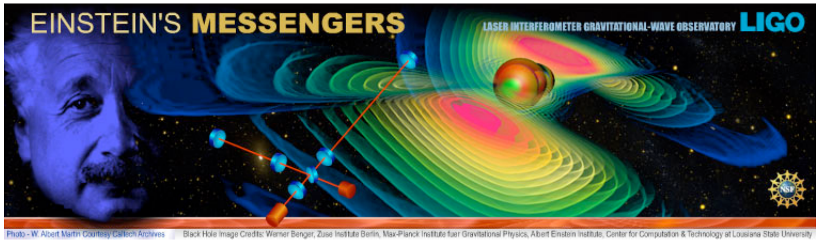

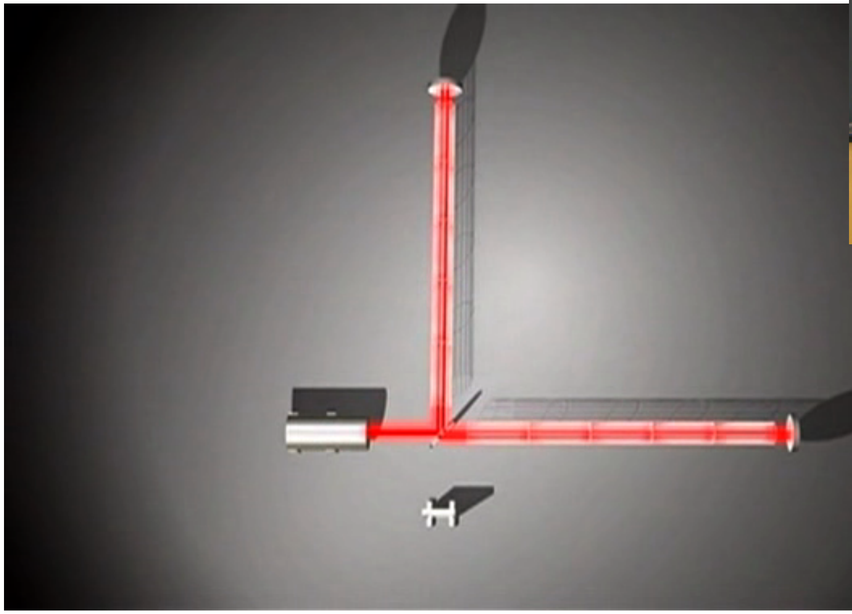

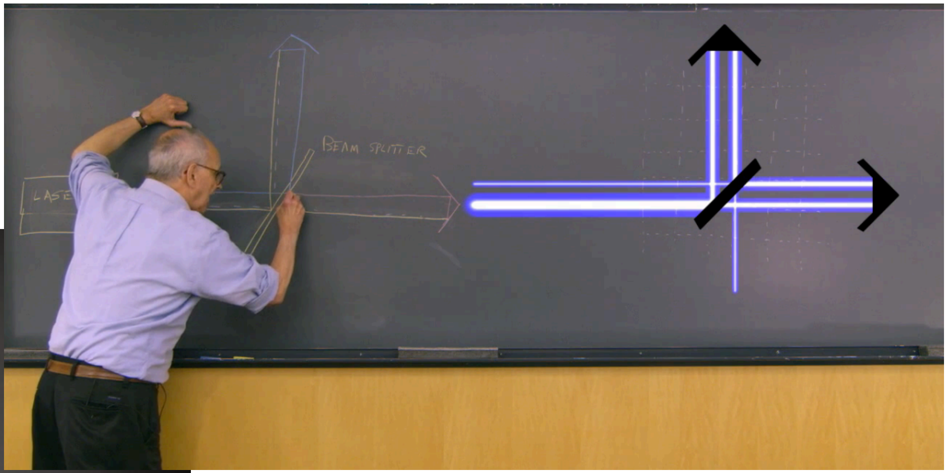

“LIGO generations”
http://www.kaistaats.com/film/ligo-generations/

Einstein’s messengers,
National Science Foundation video

http://www.einsteinsmessengers.org/

Pulsar timing

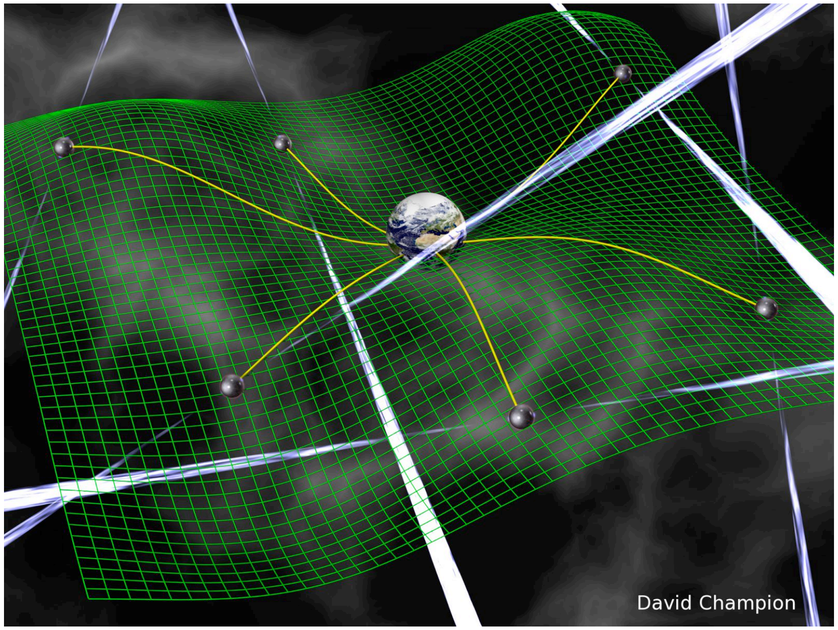
David Champion

Measuring changes in phase of pulsar radio beams on Earth, we have a “galactic scale interferometer” measuring gravitational waves with periods of several years (nHz frequencies): mergers of super-massive black holes (galaxies!). They are limited by noise in the time of arrival of radio beams, number of pulsars and integration time.

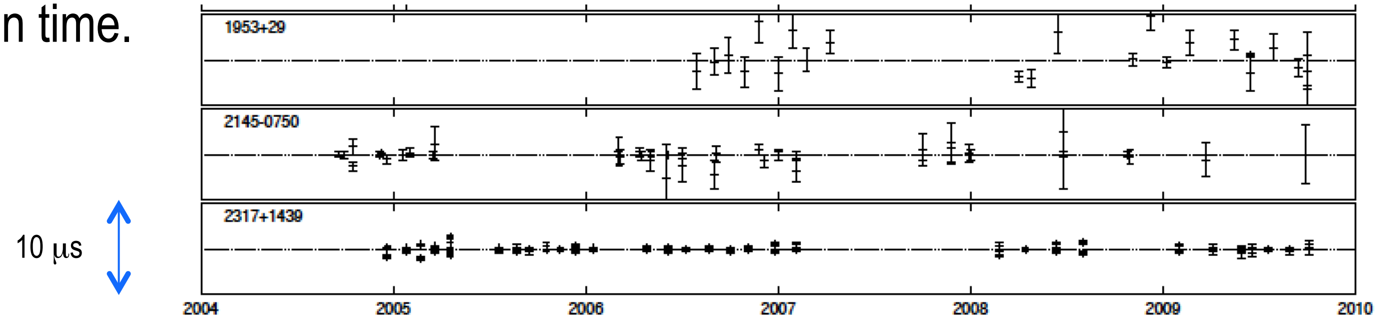

Pulsar timing results

NASA/JPL-Caltech/GSFC

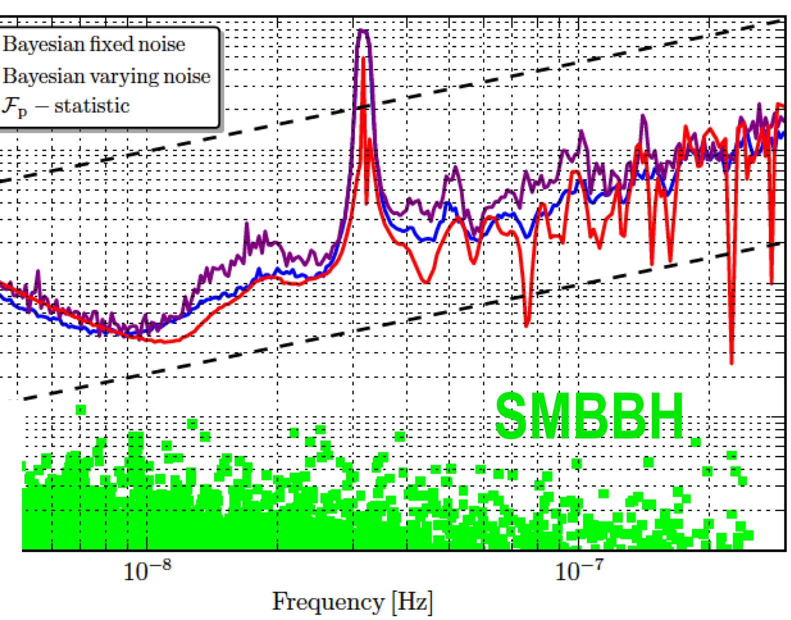

Z. Arzoumanian et al (NANOGrav collaboration), 2014 *Astrophys. J.* **794** 141

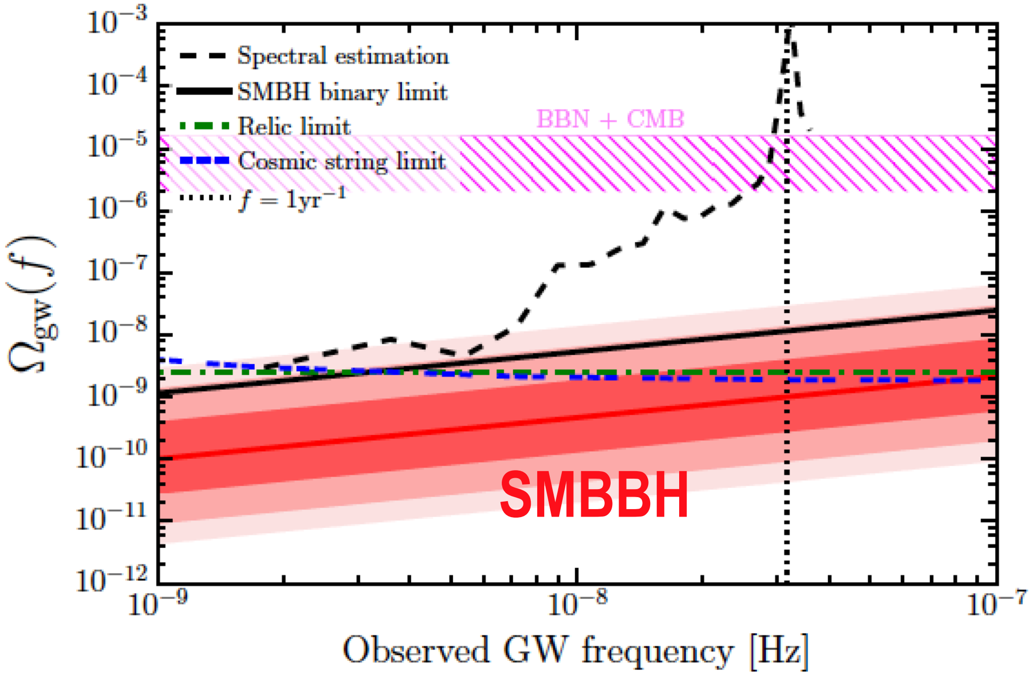

Lentati et al, (EPTA collaboration), arXiv:1504.03692

GW PTA detections are coming soon

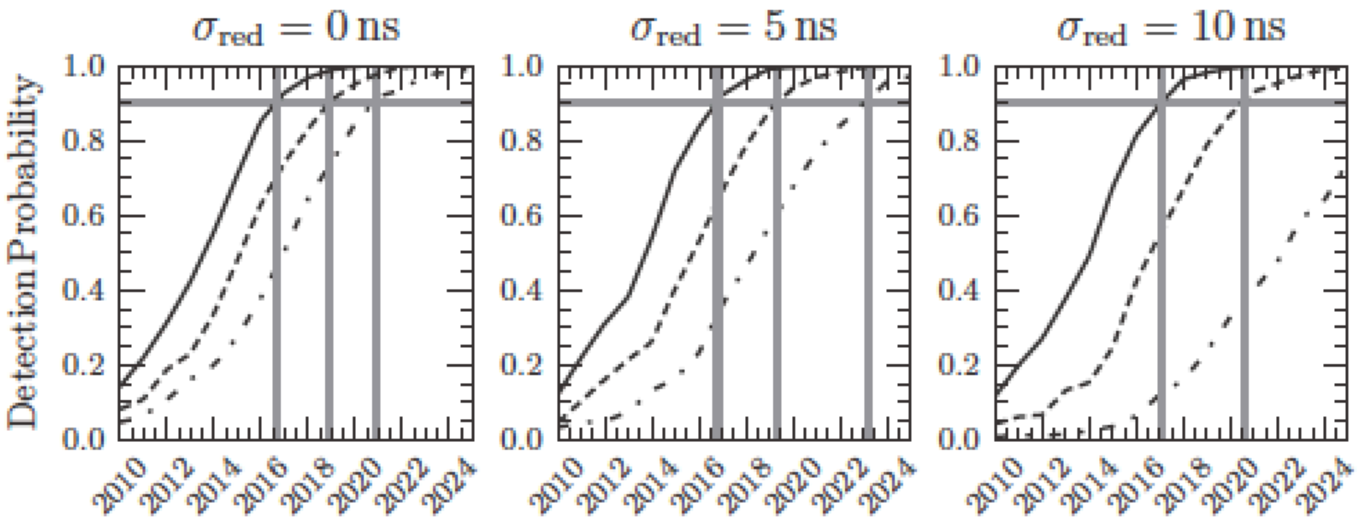

Figure 4. Detection probability versus time in years for the NANOGrav PTA. We show the detection probability for three different amplitudes $A = 5.6 \times 10^{-16}$ (dash–dot), $A = 1 \times 10^{-15}$ (dashed), and $A = 2 \times 10^{-15}$ (solid) of the stochastic background generated by SMBBHs [7]. We have used the combined epoch RMSs of the 17 pulsars in [26], started timing 35 total pulsars in 2013, and added 3 new pulsars per year with an epoch combined RMS of 200 ns prior to hardware improvements (this is the median of the 17 pulsars in [26]).

Siemens et al., Class. Quantum Grav. 30 (2013) 224015

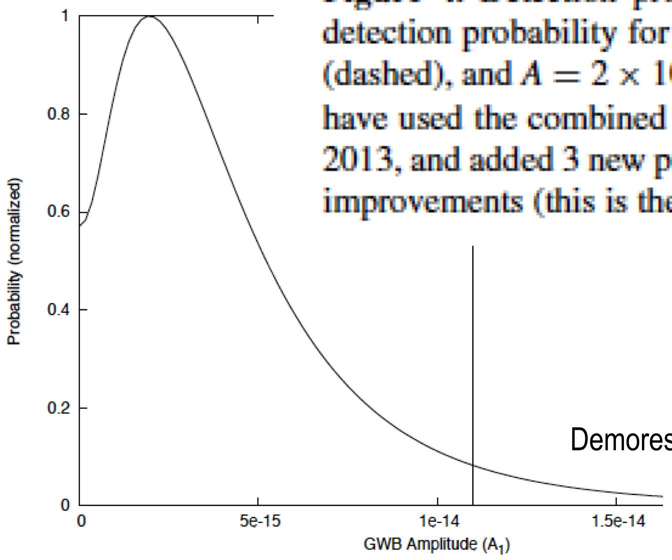

Demorest et al. (NANOggrav), ApJ 762, 94(1/2013)

Space-based detector: (e)LISA

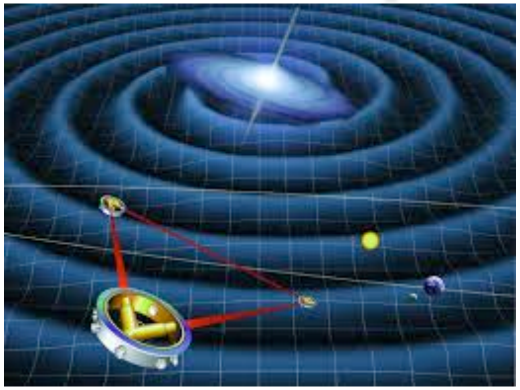

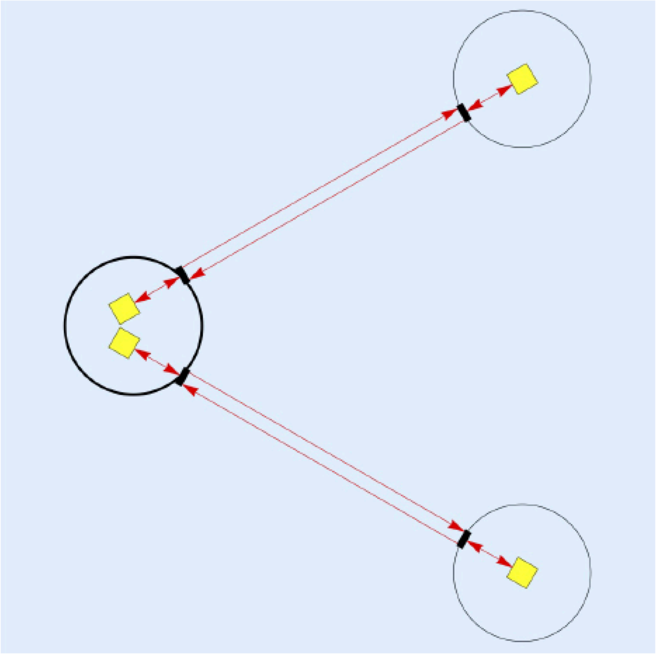

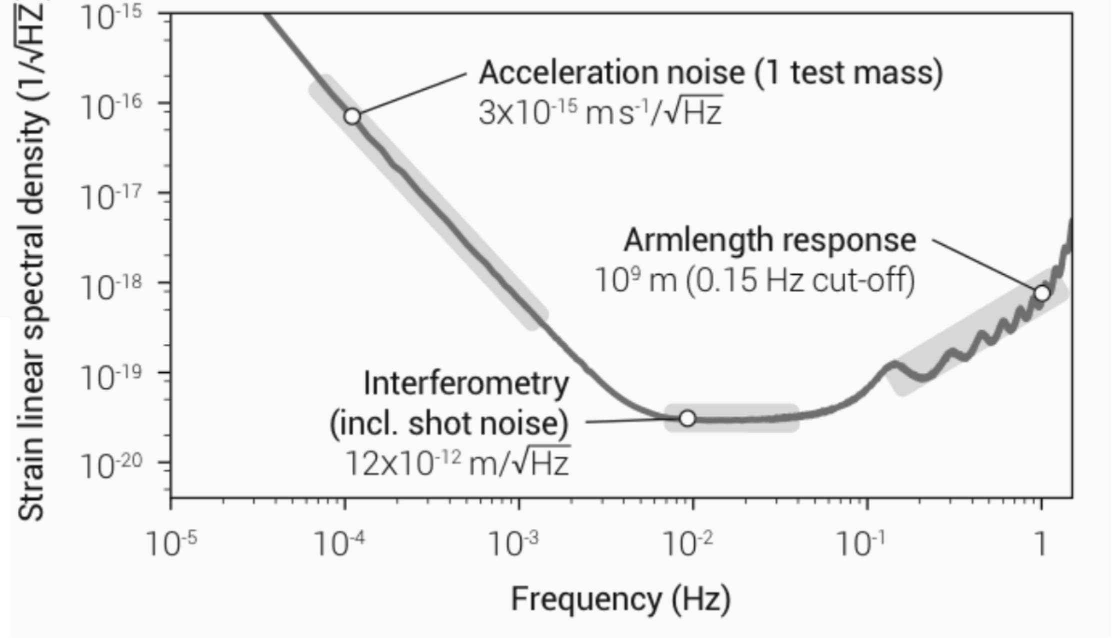

eLISA white paper

eLISA: ESA large L3 mission, launch date 2034,
Mission design call 2022 (or 2016?)

LISA Pathfinder

Image Credits: Airbus Defence & Space, ESA

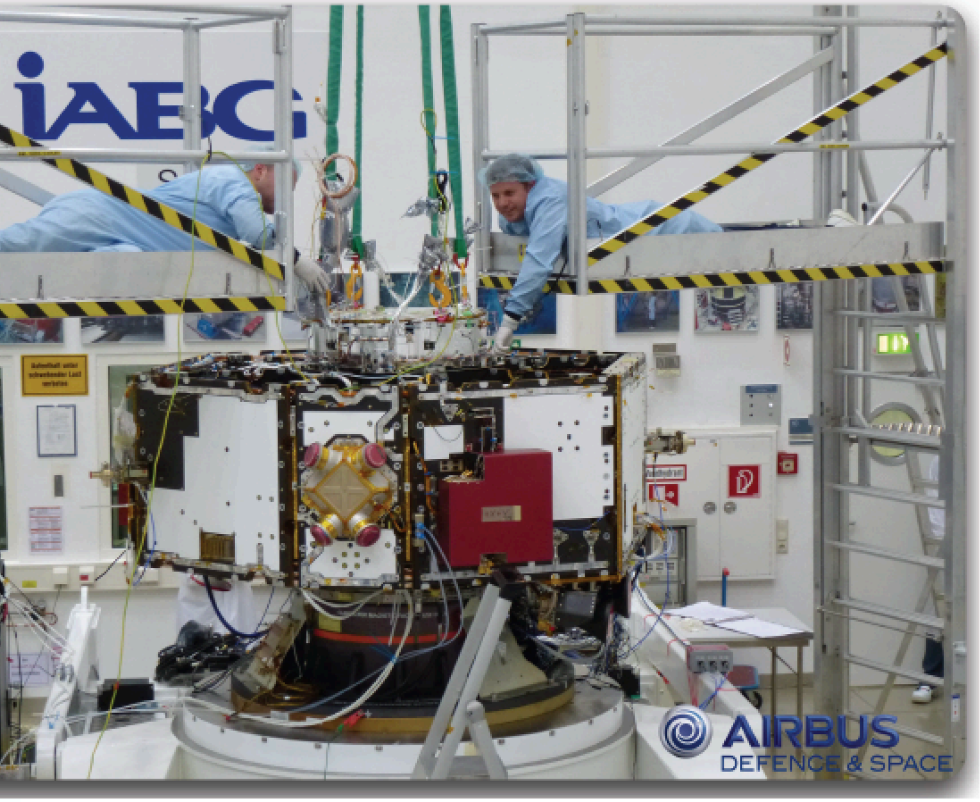

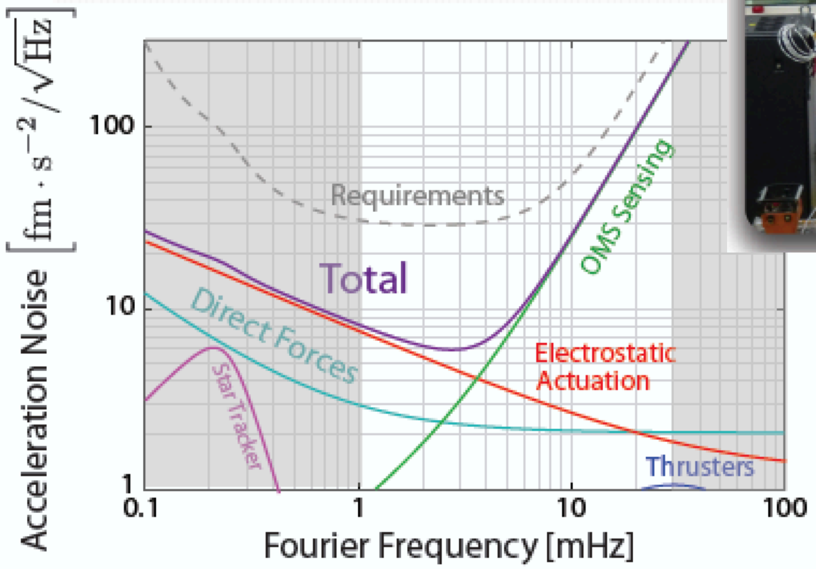

Launch date October 2015!

LISA Science

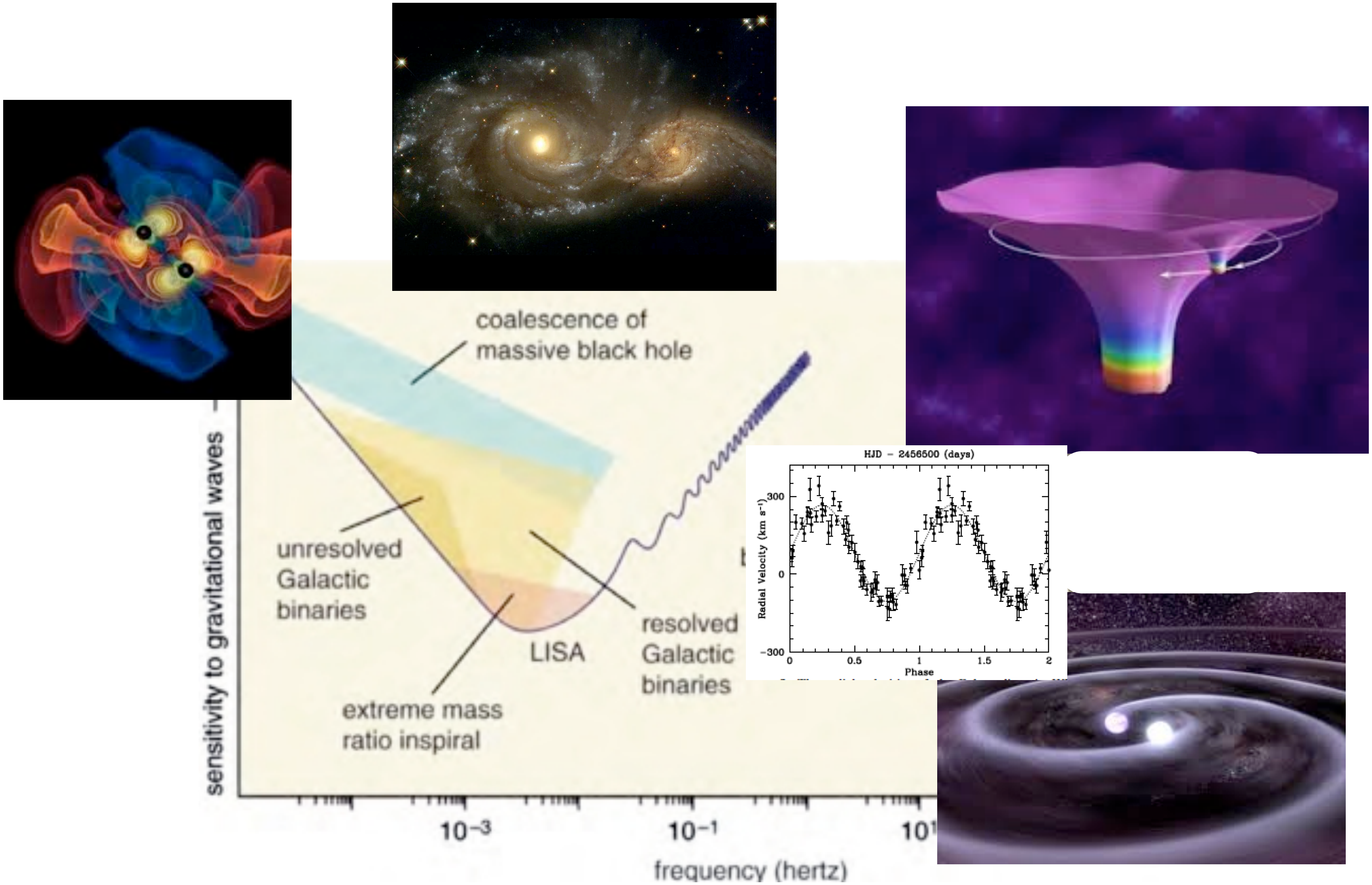

Very incomplete history of LIGO GW detectors

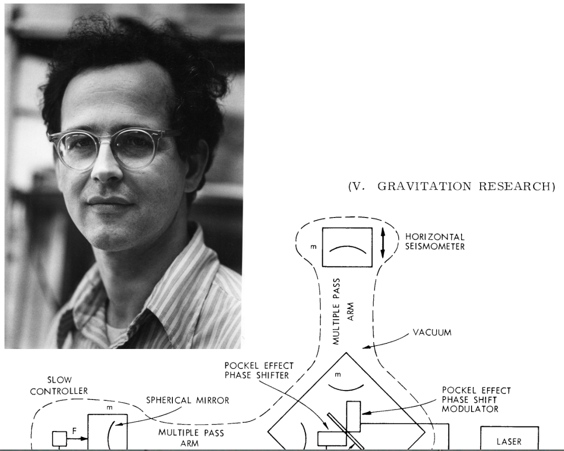

A STUDY OF A LONG BASELINE

GRAVITATIONAL WAVE ANTENNA SYSTEM

Prepared for the National Science Foundation
under NSF Grant PHY-8109581
to the Massachusetts Institute of Technology

Prepared By:

Paul Linsay	MIT
Peter Saulson	MIT
Rainer Weiss	MIT

With Contributions By:

Stan Whitcomb	CalTech

Industrial Consultants:

Arthur D. Little Corporation	Cambridge, Massachusetts
Stone & Webster Engineering Corporation	Boston, Massachusetts

OCTOBER 1983

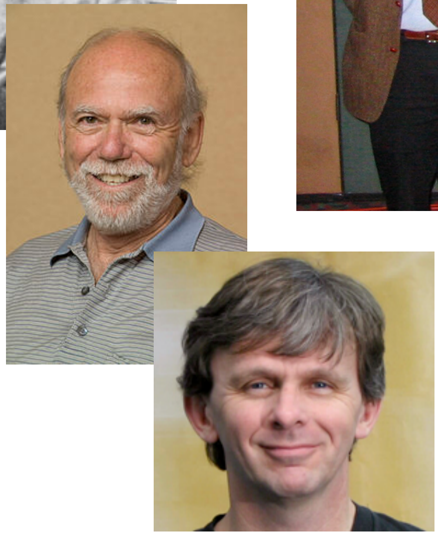

LIGO today

LIGO Scientific Collaboration

900+ members, 80+ institutions, 16 countries

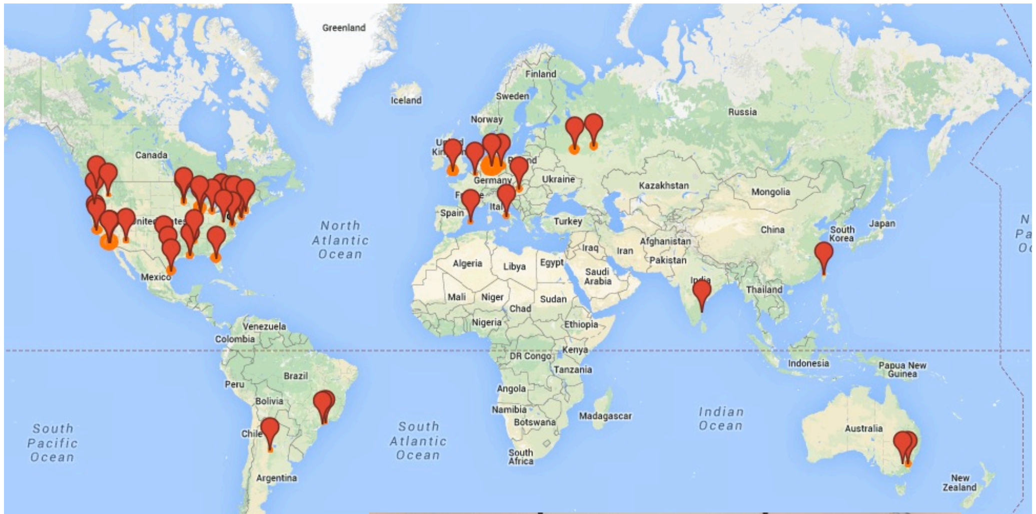

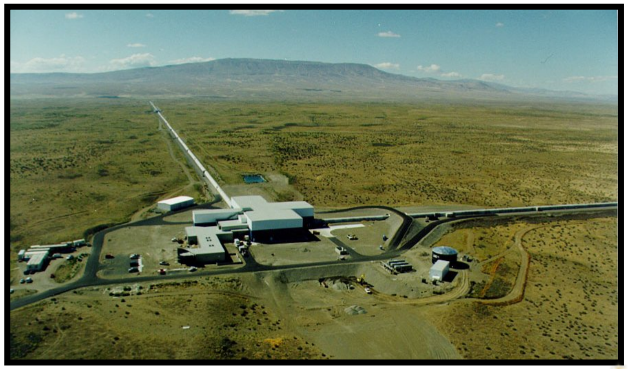

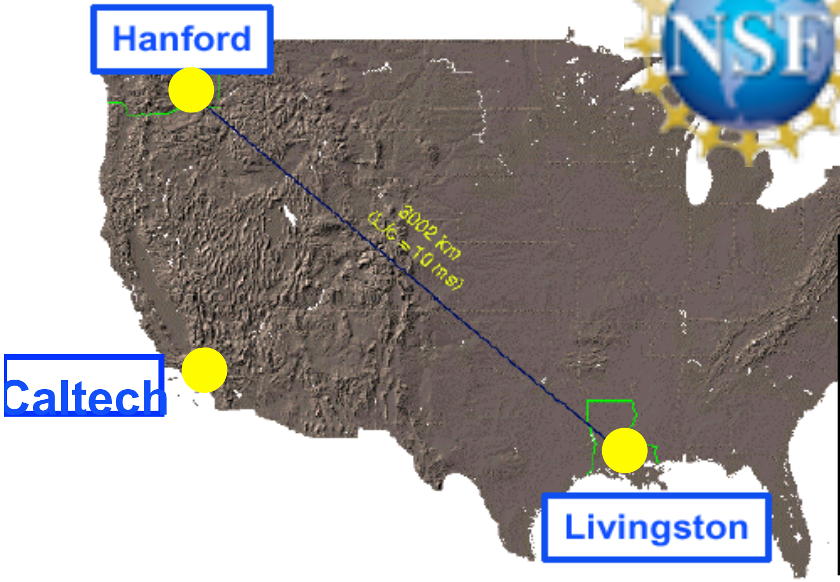

Ground Based Detectors: 2005-2010

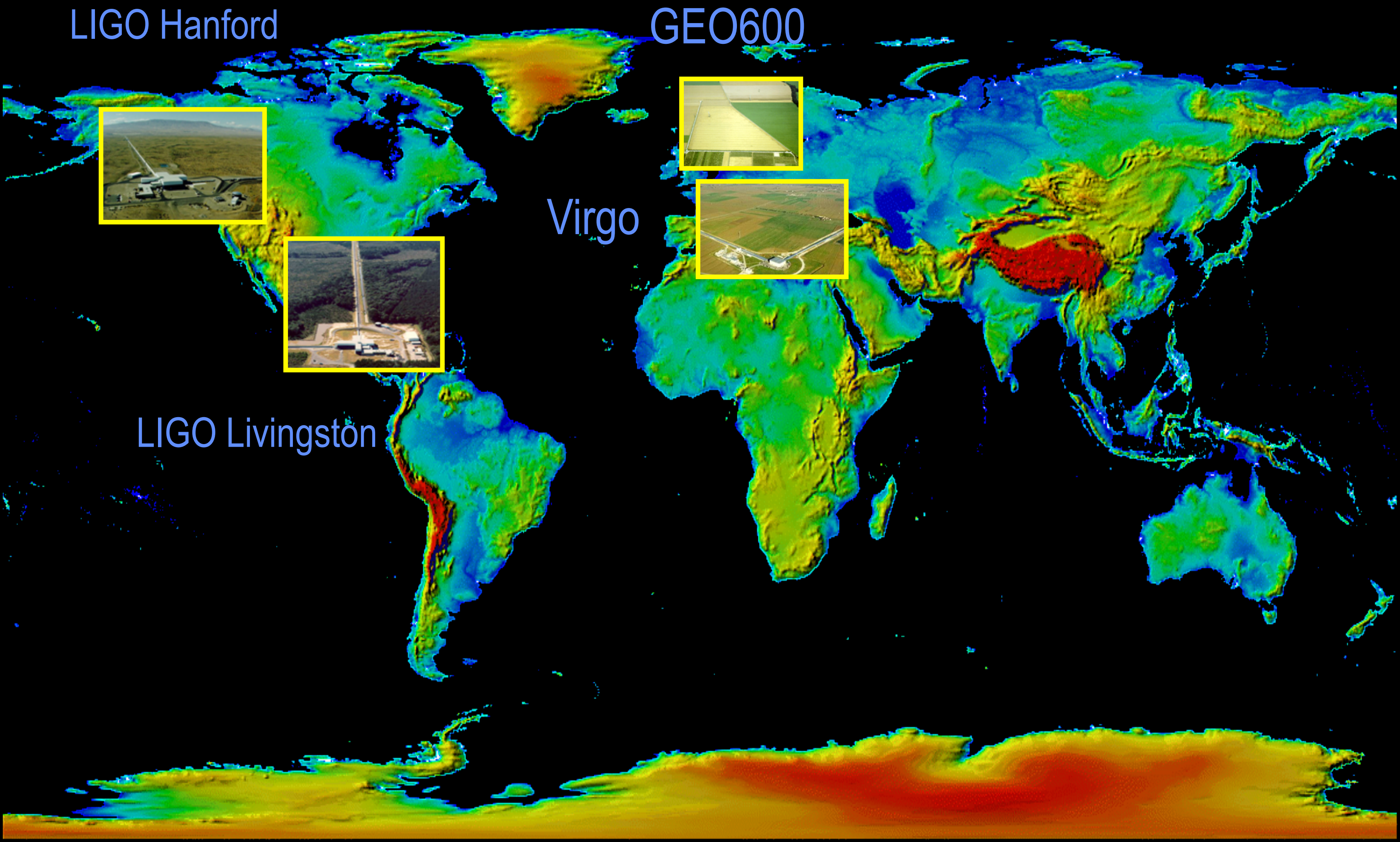

LIGO GW Searches 2005-2010

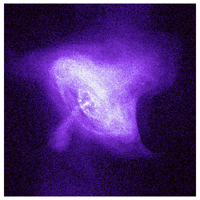

Crab pulsar (NASA, Chandra Observatory)

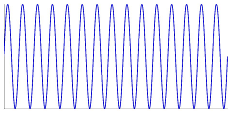

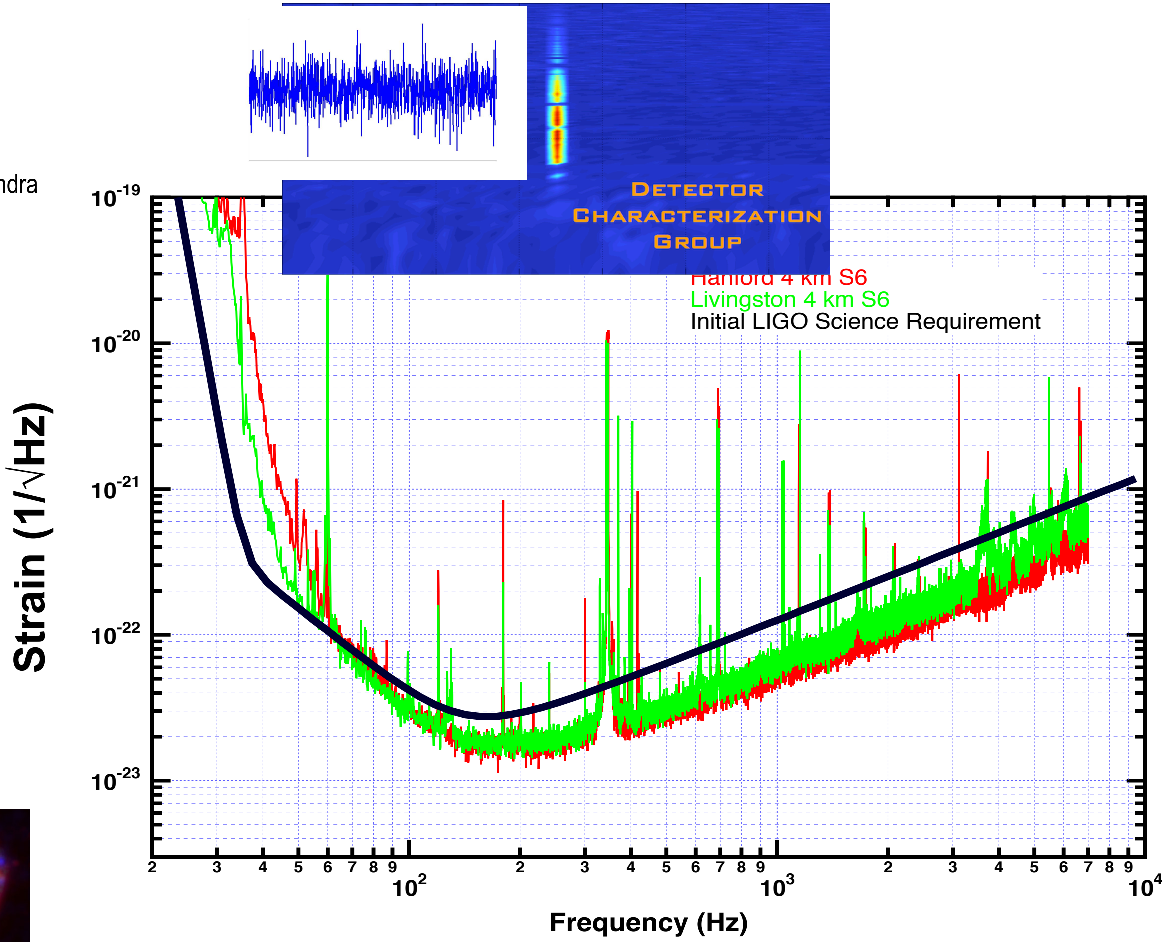

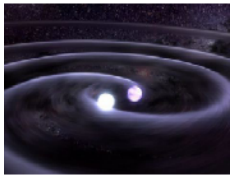

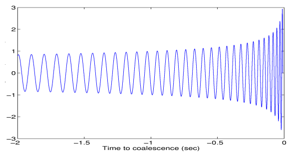

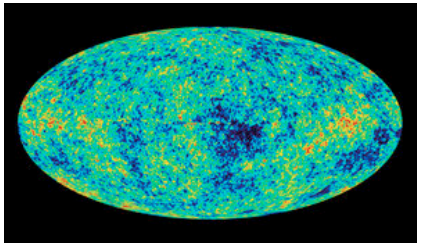

NASA, WMAP

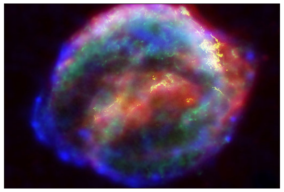

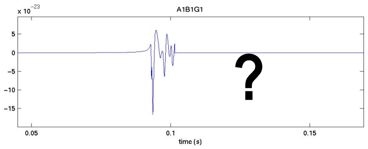

LIGO-T1400054

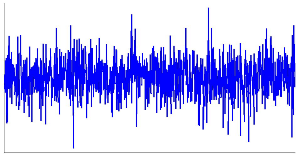

www.ligo.org

LIGO-Virgo detectors 2005-2010

Astrophys. J. **681** (2008) 1419

Average range for a binary neutron star system (with m=1.4 solar masses)

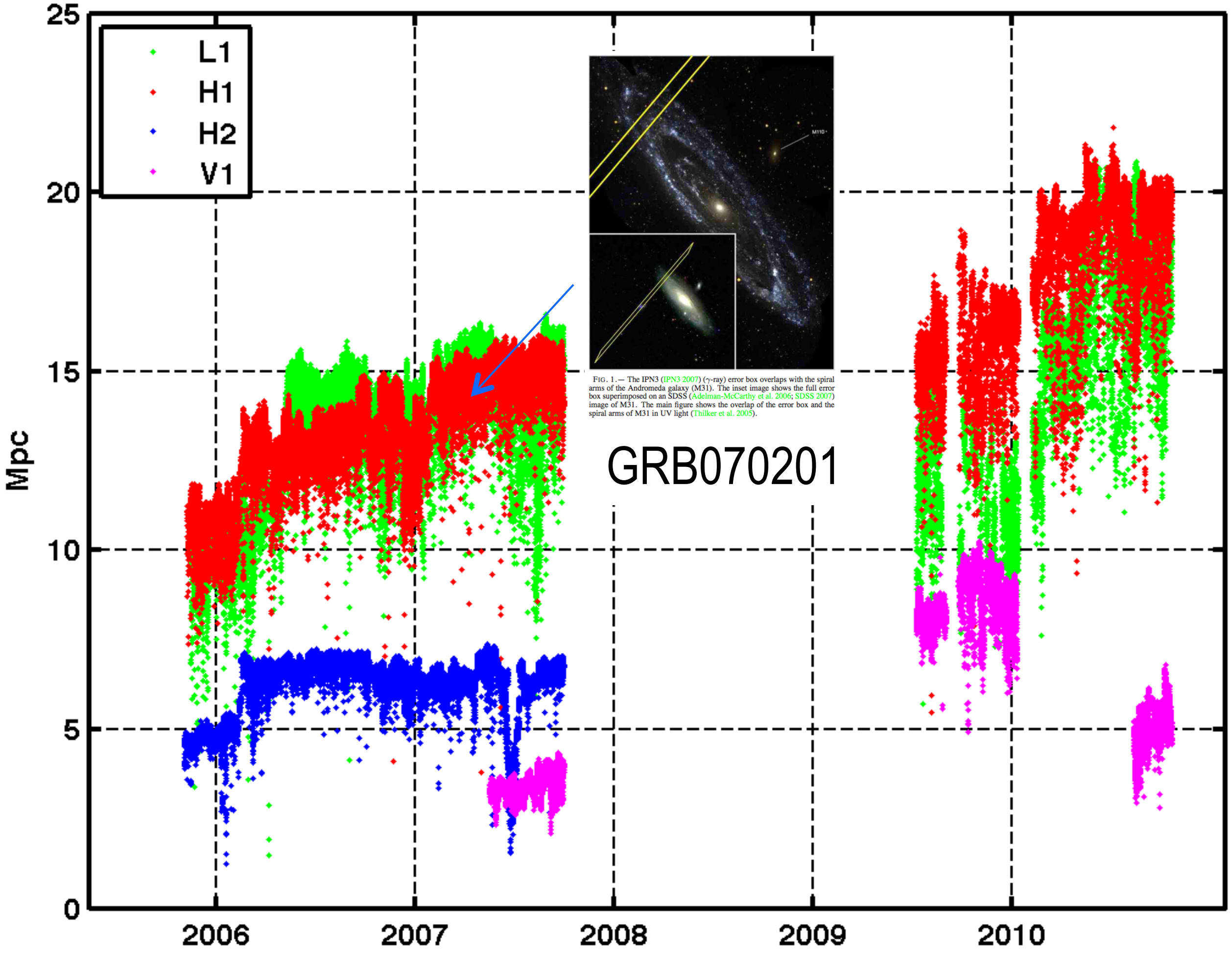

FIG. 1.— The IPN3 (IPN3 2007) (γ-ray) error box overlaps with the spiral arms of the Andromeda galaxy (M31). The inset image shows the full error box superimposed on an SDSS (Adelman-McCarthy et al. 2006; SDSS 2007) image of M31. The main figure shows the overlap of the error box and the spiral arms of M31 in UV light (Thilker et al. 2005).

GRB070201

Some interesting results 2005-2011

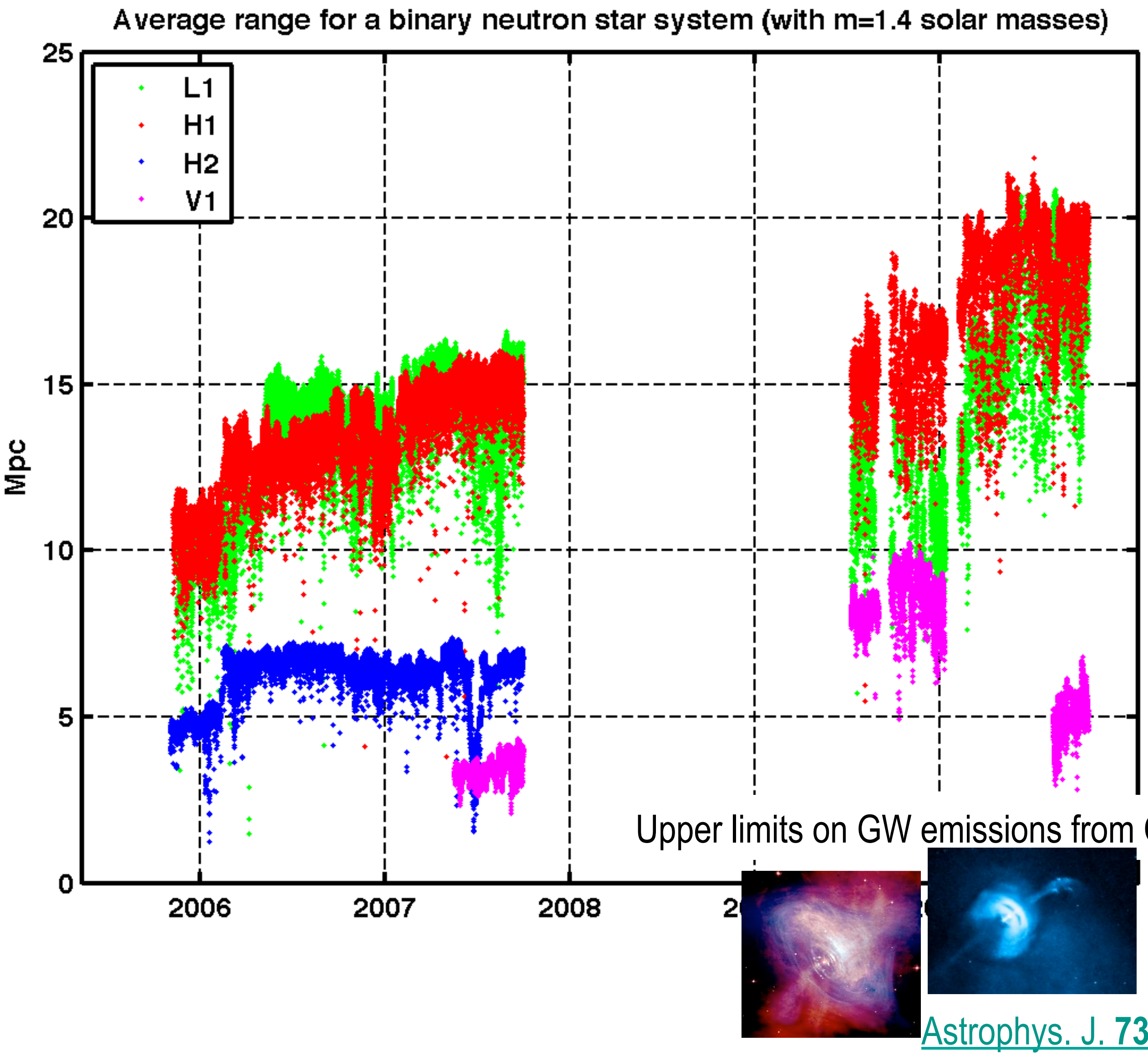

Upper limits on GW emissions from Crab and Vela pulsars

Astrophys. J. **737** (2011) 93

Astrophys. J. **722** (2010) 1504

Some interesting results 2005-2011

Upper limit on GW stochastic background

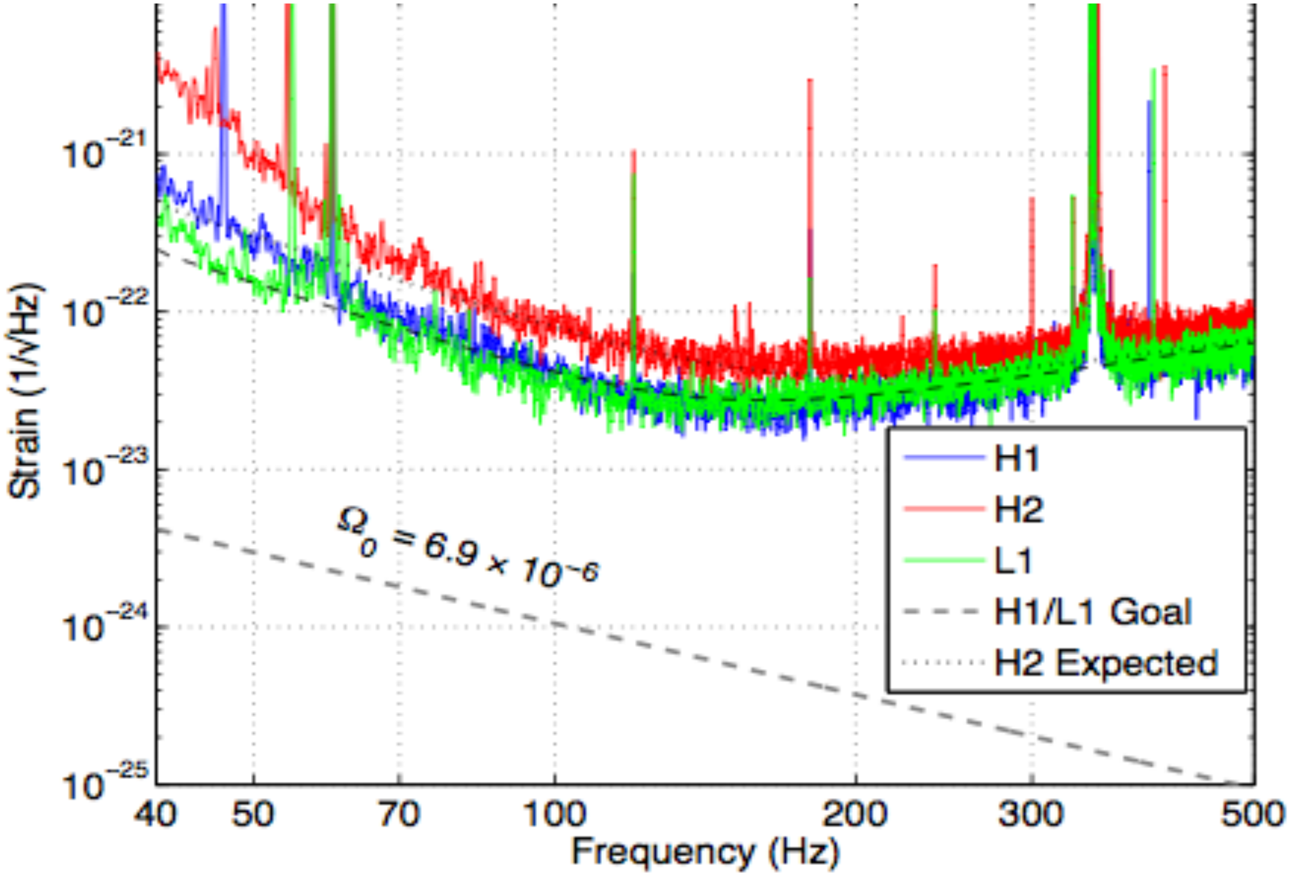

Nature **460** (2009) 990

Some interesting results 2005-2011

False alarm rate ~1/7000 yrs!

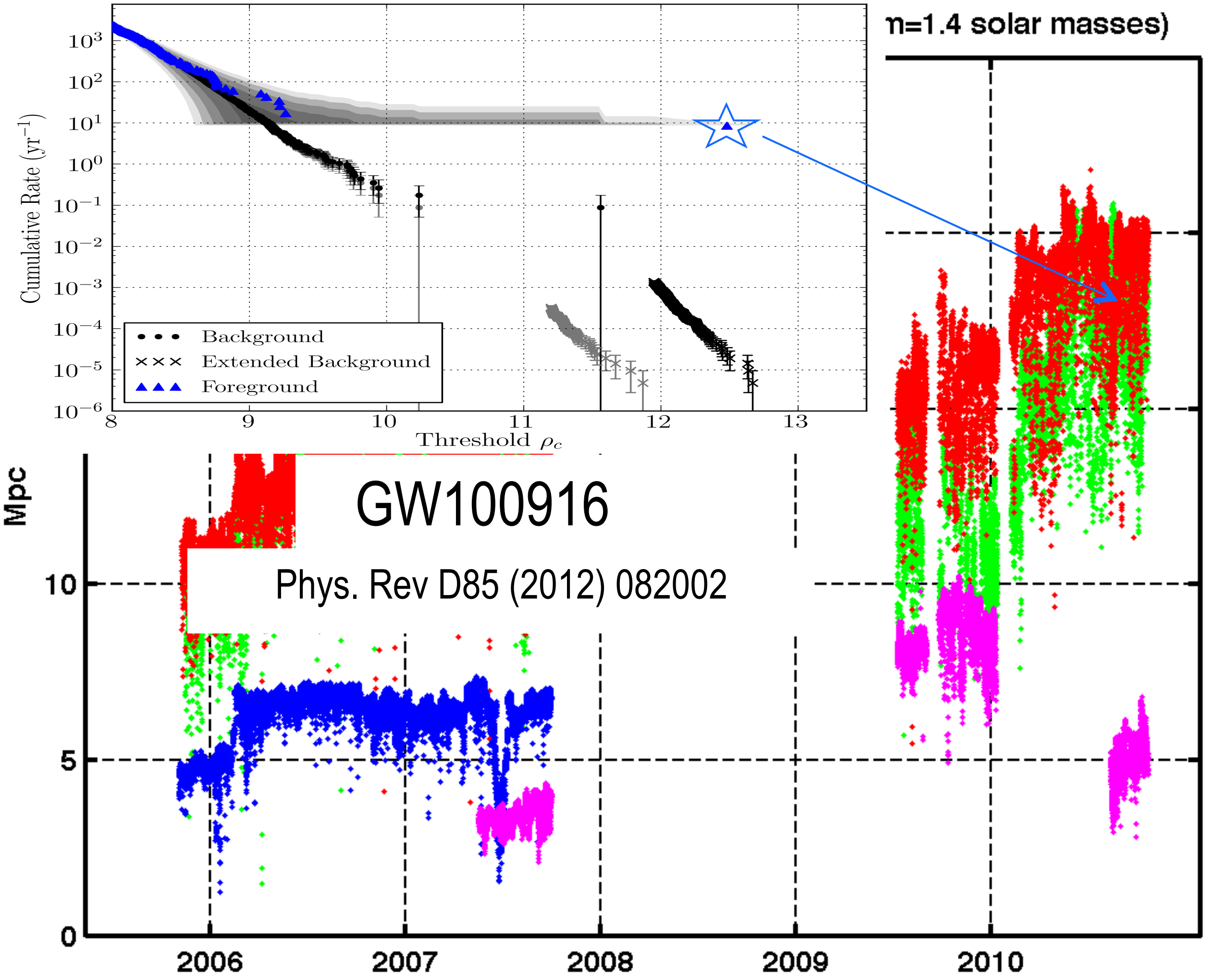

GW100916

Phys. Rev D85 (2012) 082002

Exciting experimental results too

NATURE PHOTONICS DOI: 10.1038/NPHOTON.2013.177 LETTERS

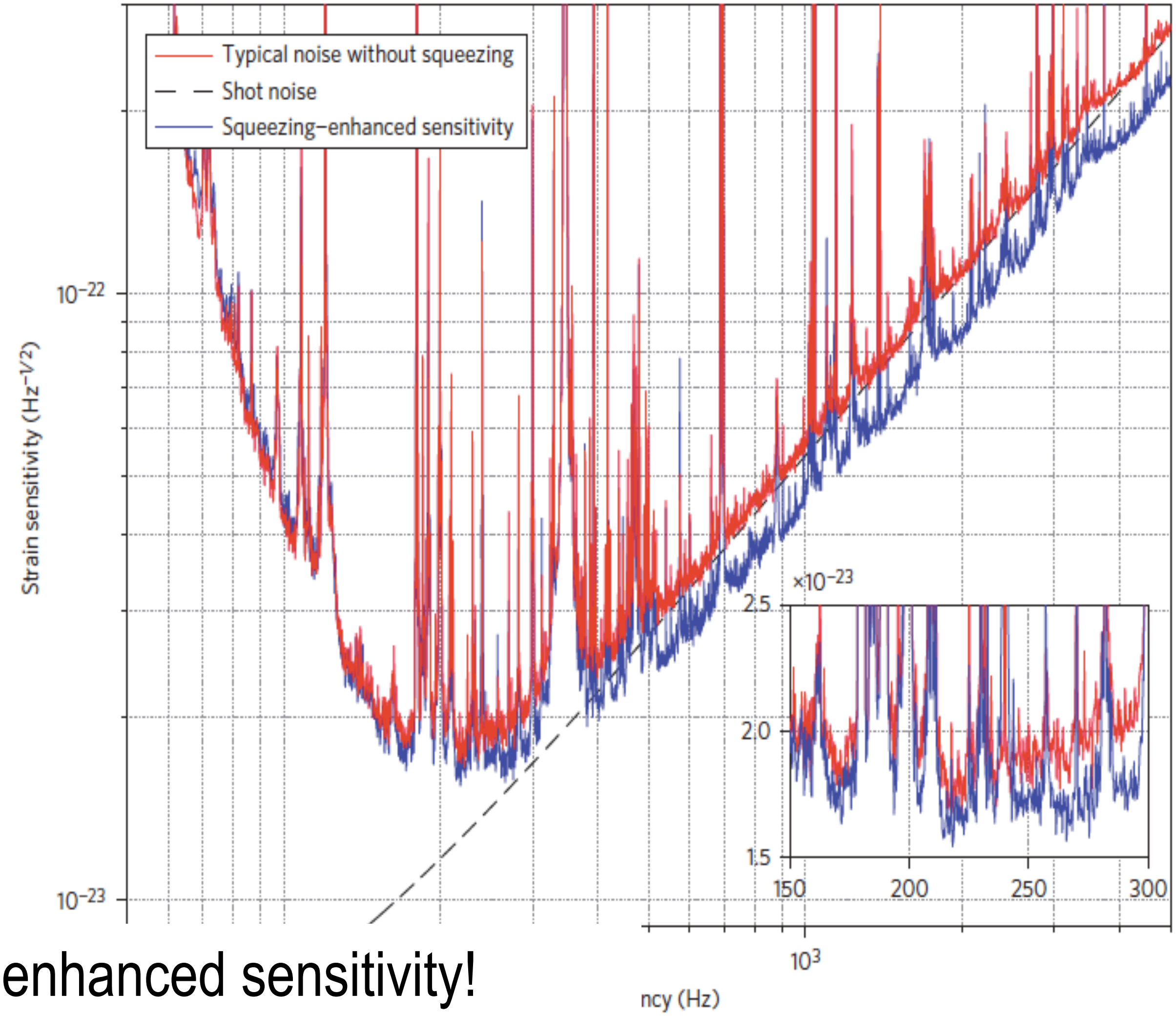

Quantum-enhanced sensitivity!

The future is here! Advanced LIGO

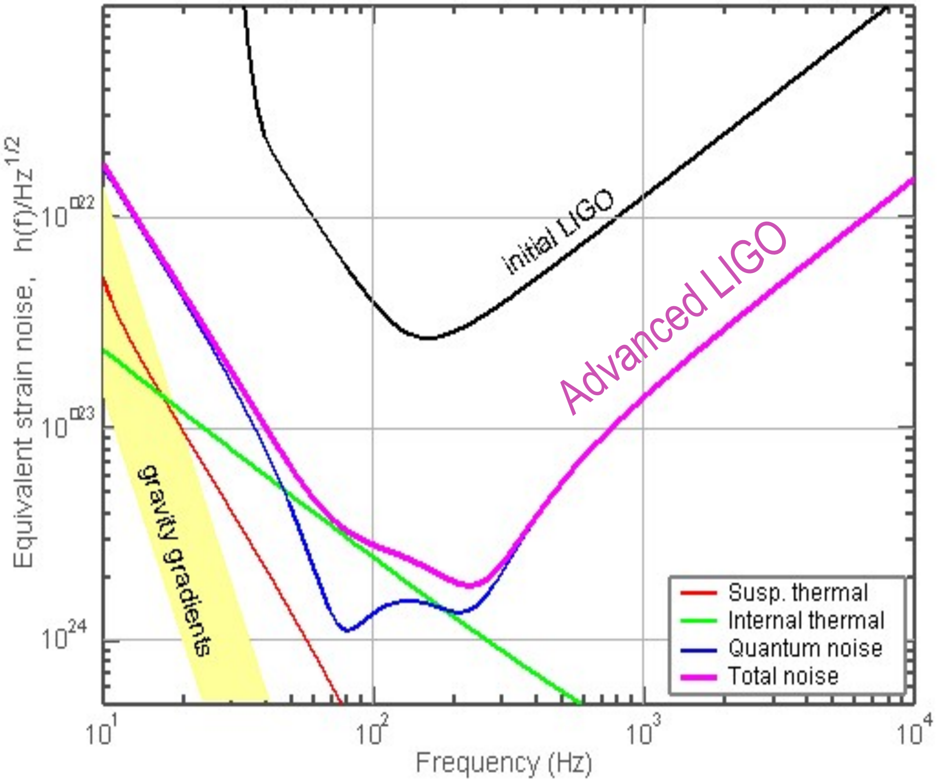

~10 times better than initial LIGO
First observing run starting this year (!!)
with increasing sensitivity to follow.

Dual recycled Fabry-Perot Michelson interferometer

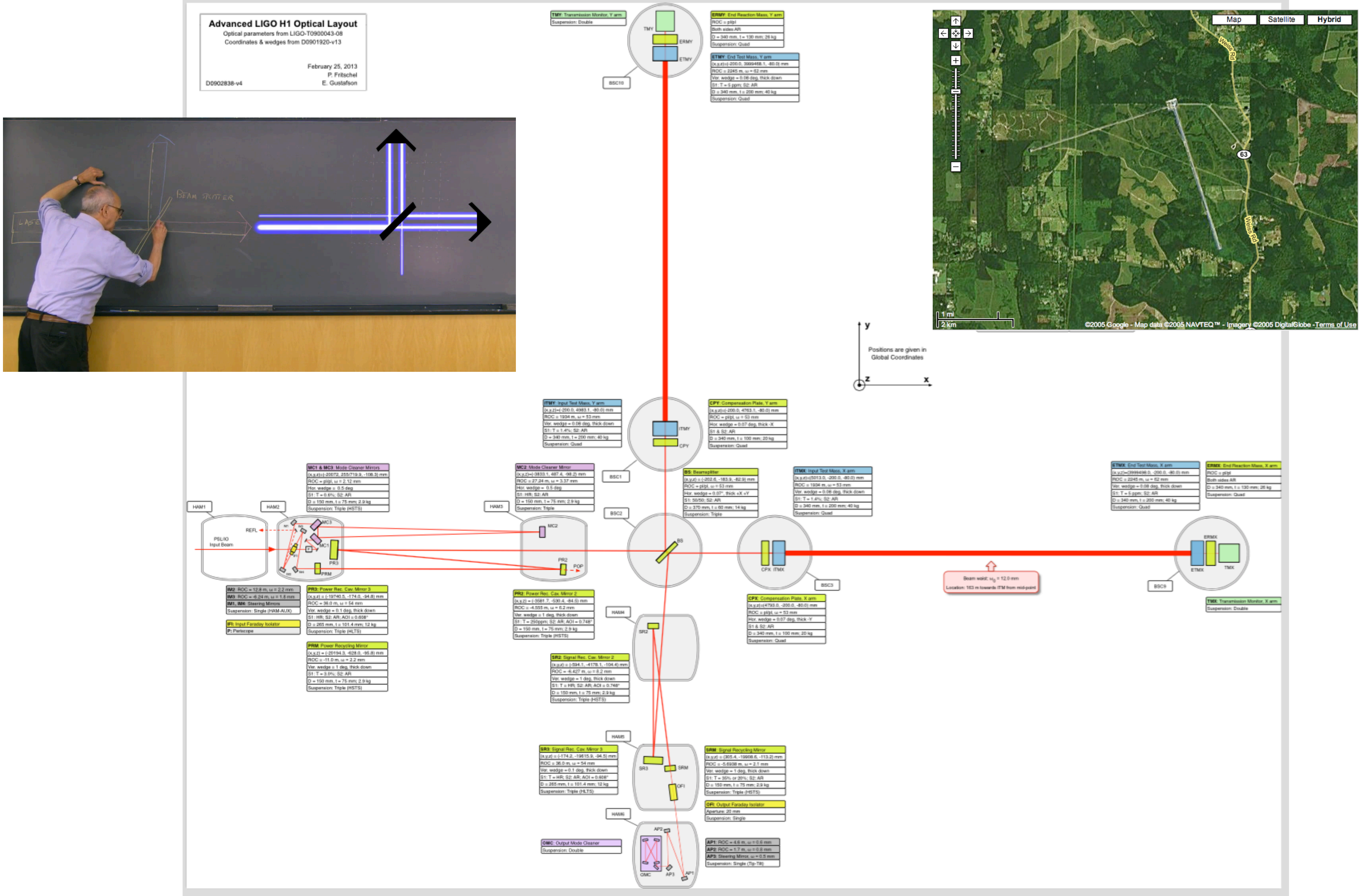

Advanced LIGO H1 Optical Layout
Optical parameters from LIGO-T0900043-08
Coordinates & wedges from D0901920-v13

February 25, 2013
P. Fritschel
E. Gustafson
D0902838-v4

TMY: Transmission Monitor, Y arm
Suspension: Double

ERMY: End Reaction Mass, Y arm
ROC = pl/pl
Both sides AR
D = 340 mm, t = 130 mm; 26 kg
Suspension: Quad

ETMY: End Test Mass, Y arm
(x,y,z)=(-200.0, 3999468.1, -80.0) mm
ROC = 2245 m, ω = 62 mm
Ver. wedge = 0.08 deg, thick down
S1: T = 5 ppm; S2: AR
D = 340 mm, t = 200 mm; 40 kg
Suspension: Quad

Positions are given in Global Coordinates

ITMY: Input Test Mass, Y arm
(x,y,z)=(-200.0, 4983.1, -80.0) mm
ROC = 1934 m, ω = 53 mm
Ver. wedge = 0.08 deg, thick down
S1: T = 1.4%; S2: AR
D = 340 mm, t = 200 mm; 40 kg
Suspension: Quad

CPY: Compensation Plate, Y arm
(x,y,z)=(-200.0, 4763.1, -80.0) mm
ROC = pl/pl, ω = 53 mm
Hor. wedge = 0.07 deg, thick -X
S1 & S2: AR
D = 340 mm, t = 100 mm; 20 kg
Suspension: Quad

MC1 & MC3: Mode Cleaner Mirrors
(x,y,z)=(-20072, 255/719.9, -108.3) mm
ROC = pl/pl, ω = 2.12 mm
Hor. wedge = 0.5 deg
S1: T = 0.6%; S2: AR
D = 150 mm, t = 75 mm; 2.9 kg
Suspension: Triple (HSTS)

MC2: Mode Cleaner Mirror
(x,y,z)=(-3833.1, 487.4, -98.2) mm
ROC = 27.24 m, ω = 3.37 mm
Hor. wedge = 0.5 deg
S1: HR; S2: AR
D = 150 mm, t = 75 mm; 2.9 kg
Suspension: Triple

BS: Beamsplitter
(x,y,z) = (-202.6, -183.9, -82.9) mm
ROC = pl/pl, ω = 53 mm
Hor. wedge = 0.07°, thick +X +Y
S1: 50/50; S2: AR
D = 370 mm, t = 60 mm; 14 kg
Suspension: Triple

ITMX: Input Test Mass, X arm
(x,y,z)=(5013.0, -200.0, -80.0) mm
ROC = 1934 m, ω = 53 mm
Ver. wedge = 0.08 deg, thick down
S1: T = 1.4%; S2: AR
D = 340 mm, t = 200 mm; 40 kg
Suspension: Quad

ETMX: End Test Mass, X arm
(x,y,z)=(3999498.0, -200.0, -80.0) mm
ROC = 2245 m, ω = 62 mm
Ver. wedge = 0.08 deg, thick down
S1: T = 5 ppm; S2: AR
D = 340 mm, t = 200 mm; 40 kg
Suspension: Quad

ERMX: End Reaction Mass, X arm
ROC = pl/pl
Both sides AR
D = 340 mm, t = 130 mm; 26 kg
Suspension: Quad

Beam waist: ω_0 = 12.0 mm
Location: 163 m towards ITM from mid-point

TMX: Transmission Monitor, X arm
Suspension: Double

CPX: Compensation Plate, X arm
(x,y,z)=(4793.0, -200.0, -80.0) mm
ROC = pl/pl, ω = 53 mm
Hor. wedge = 0.07 deg, thick -Y
S1 & S2: AR
D = 340 mm, t = 100 mm; 20 kg
Suspension: Quad

IM2: ROC = 12.8 m, ω = 2.2 mm
IM3: ROC = -6.24 m, ω = 1.8 mm
IM1, IM4: Steering Mirrors
Suspension: Single (HAM-AUX)

IFI: Input Faraday Isolator
P: Periscope

PR3: Power Rec. Cav. Mirror 3
(x,y,z) = (-19740.5, -174.0, -94.8) mm
ROC = 36.0 m, ω = 54 mm
Ver. wedge = 0.1 deg, thick down
S1: HR; S2: AR; AOI = 0.608°
D = 265 mm, t = 101.4 mm; 12 kg
Suspension: Triple (HLTS)

PRM: Power Recycling Mirror
(x,y,z) = (-20194.3, -628.0, -95.8) mm
ROC = -11.0 m, ω = 2.2 mm
Ver. wedge = 1 deg, thick down
S1: T = 3.0%; S2: AR
D = 150 mm, t = 75 mm; 2.9 kg
Suspension: Triple (HSTS)

PR2: Power Rec. Cav. Mirror 2
(x,y,z) = (-3581.7, -630.4, -84.5) mm
ROC = -4.555 m, ω = 6.2 mm
Ver. wedge = 1 deg, thick down
S1: T = 250ppm; S2: AR; AOI = 0.748°
D = 150 mm, t = 75 mm; 2.9 kg
Suspension: Triple (HSTS)

SR2: Signal Rec. Cav. Mirror 2
(x,y,z) = (-594.1, -4178.1, -104.4) mm
ROC = -6.427 m, ω = 8.2 mm
Ver. wedge = 1 deg, thick down
S1: T = HR; S2: AR; AOI = 0.748°
D = 150 mm, t = 75 mm; 2.9 kg
Suspension: Triple (HSTS)

SR3: Signal Rec. Cav. Mirror 3
(x,y,z) = (-174.2, -19615.9, -94.5) mm
ROC = 36.0 m, ω = 54 mm
Ver. wedge = 0.1 deg, thick down
S1: T = HR; S2: AR; AOI = 0.608°
D = 265 mm, t = 101.4 mm; 12 kg
Suspension: Triple (HLTS)

SRM: Signal Recycling Mirror
(x,y,z) = (305.4, -19908.6, -113.2) mm
ROC = -5.6938 m, ω = 2.1 mm
Ver. wedge = 1 deg, thick down
S1: T = 35% or 20%; S2: AR
D = 150 mm, t = 75 mm; 2.9 kg
Suspension: Triple (HSTS)

OFI: Output Faraday Isolator
Aperture: 20 mm
Suspension: Single

OMC: Output Mode Cleaner
Suspension: Double

AP1: ROC = 4.6 m, ω = 0.6 mm
AP2: ROC = 1.7 m, ω = 0.8 mm
AP3: Steering Mirror, ω = 0.5 mm
Suspension: Single (Tip-Tilt)

Advanced LIGO in Pictures


Pre-stabilized Laser


Active Seismic Isolation

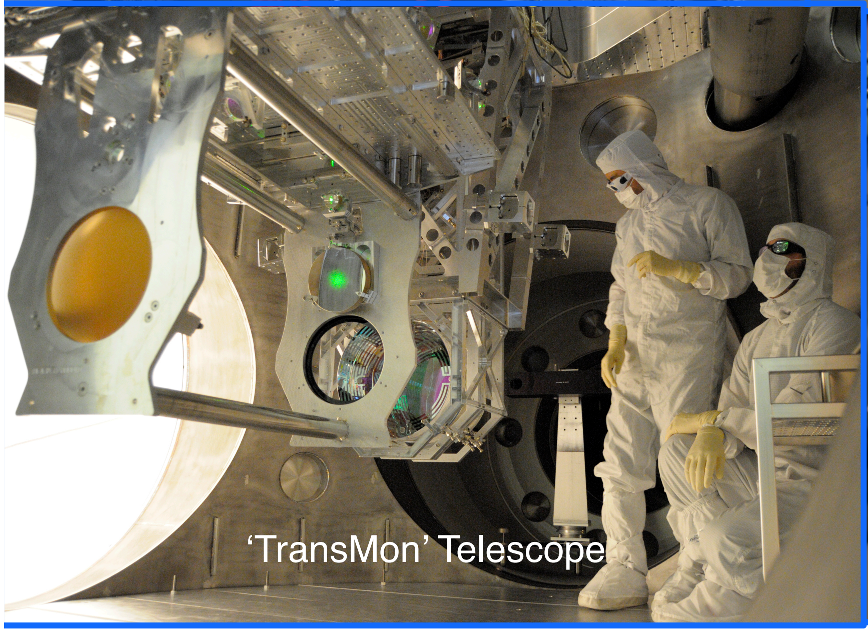
‘TransMon’ Telescope


Output Mode Cleaner

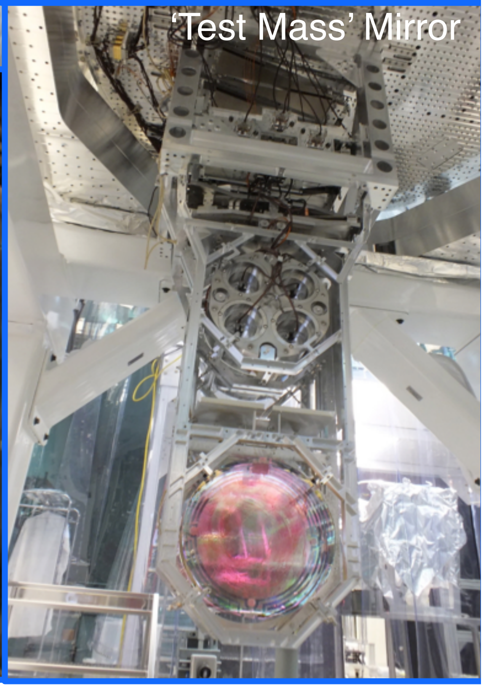
‘Test Mass’ Mirror

Current Spectra

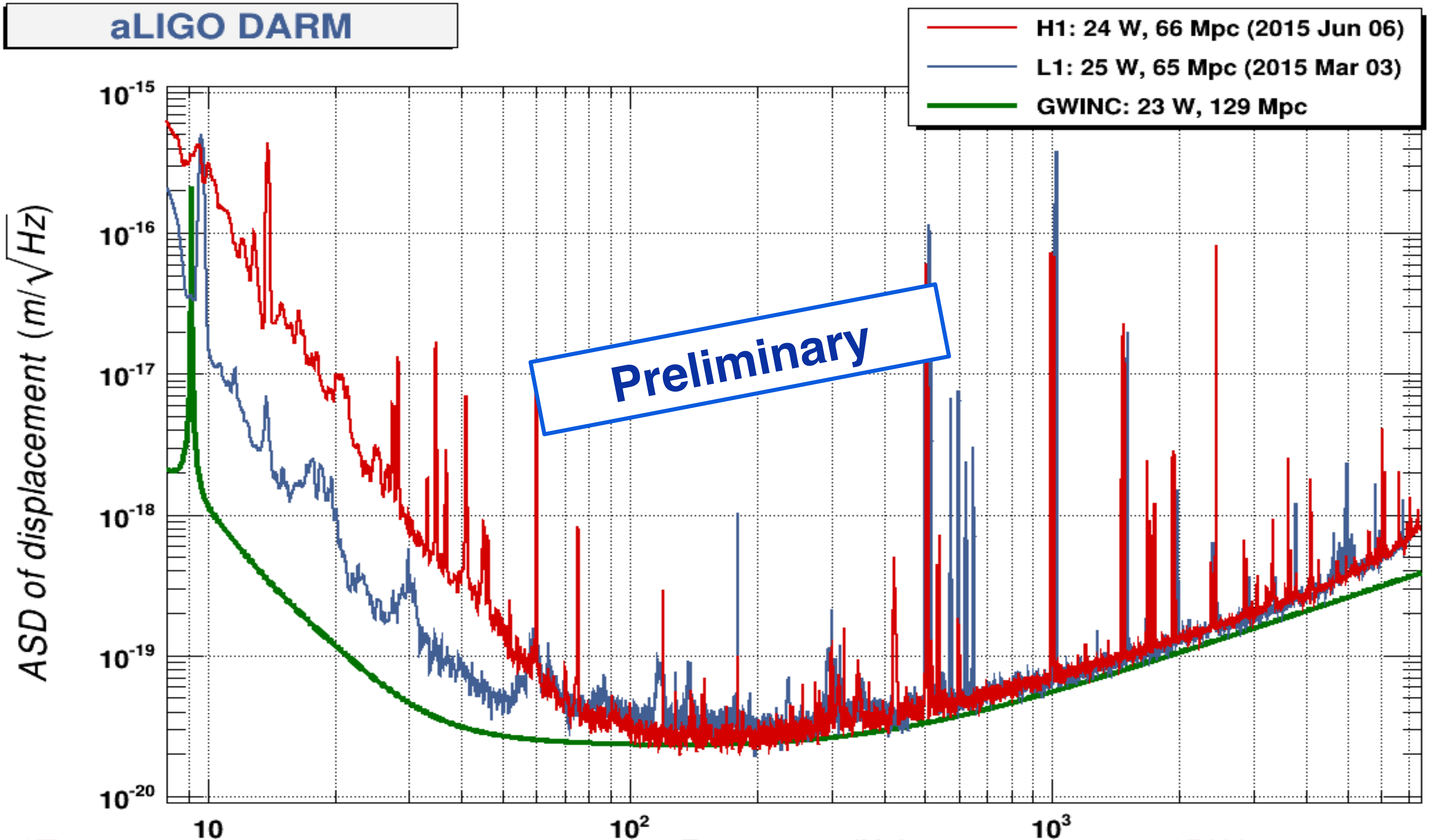

*T0=06/06/2015 04:12:40

*BW=0.187493

Engineering Run

- Stable and reliable locking of both detectors in a configuration that could be plausible during observation runs
- Best effort for similar sensitivities
- Several hours of coincidence data taking (May 26th – June 15th)
- Sufficient automation
- Hardware injections, blind injections implementation, and testing
- Includes some maintenance

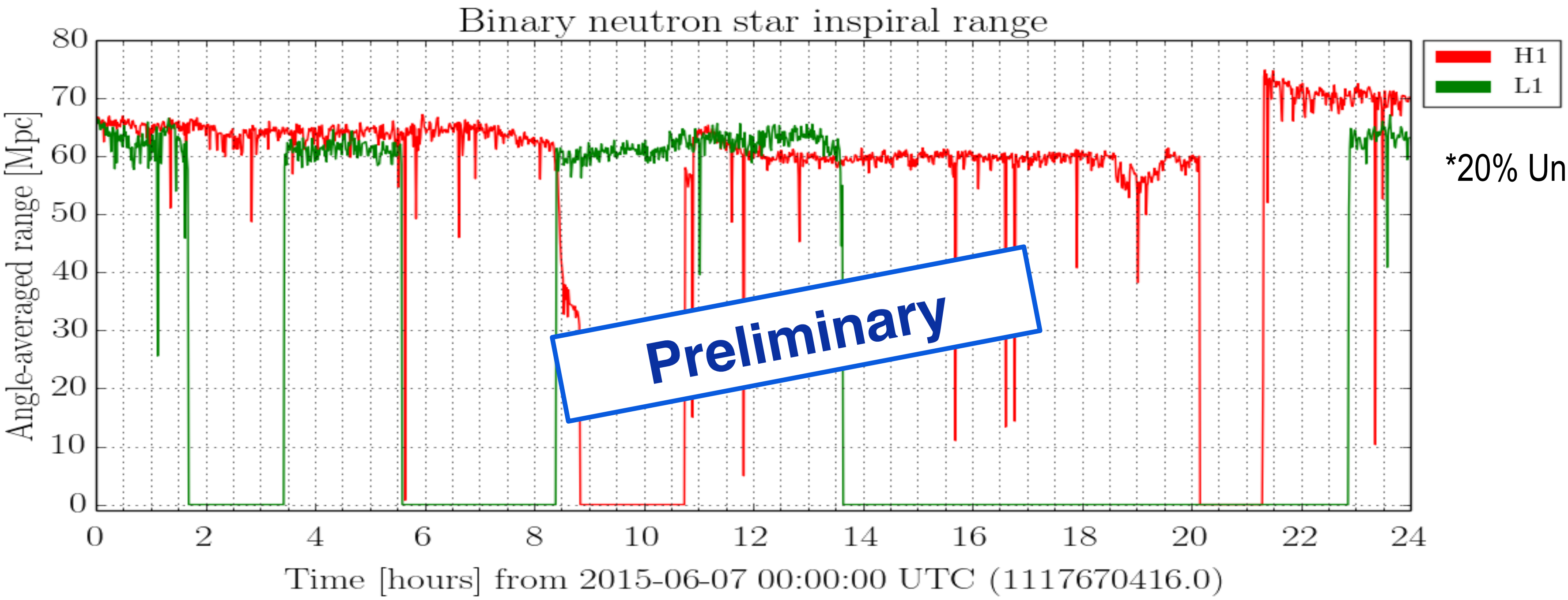

*20% Unct.

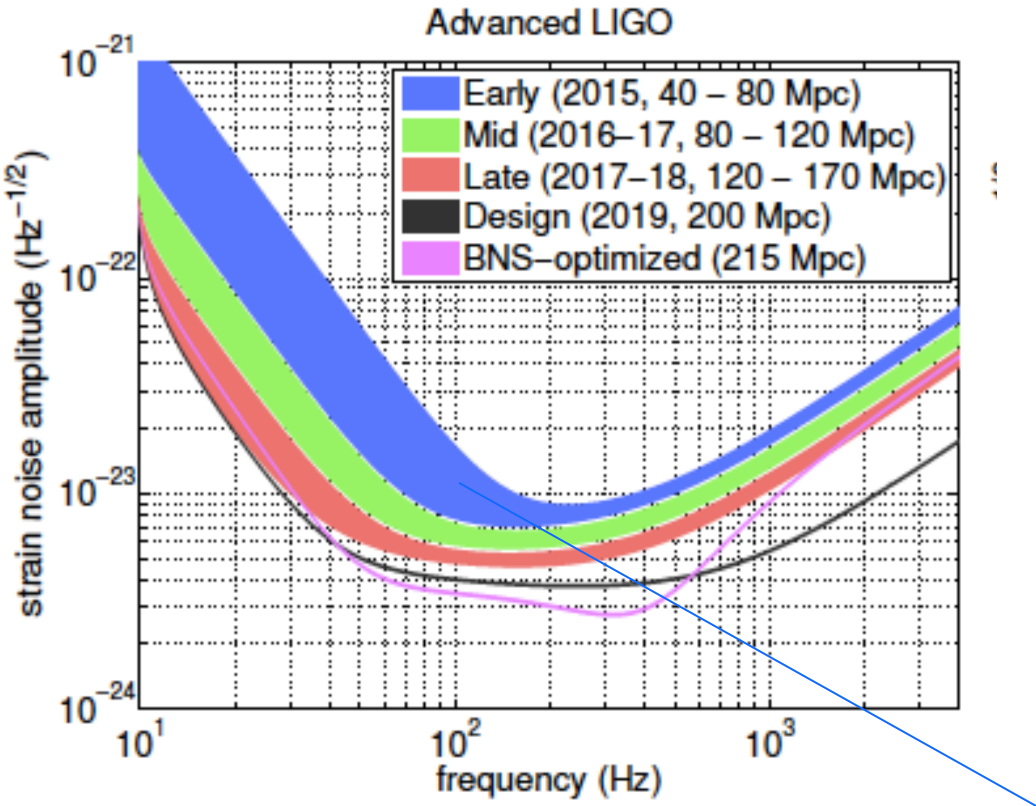

arXiv:1304.0670

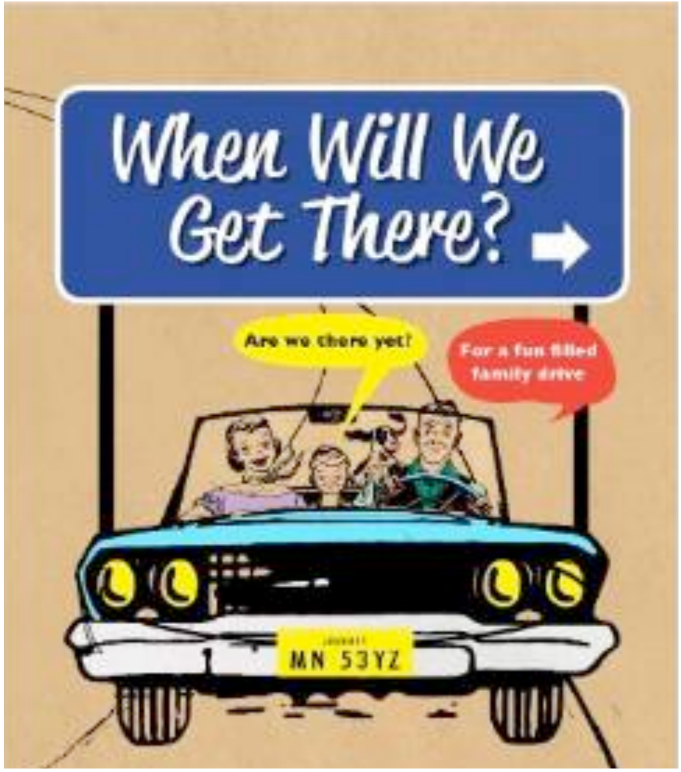

Already here!

Predictions

	Estimated Run Duration	$E_{\mathrm{GW}} = 10^{-2} M_\odot c^2$ Burst Range (Mpc)		BNS Range (Mpc)		Number of BNS Detections
Epoch		LIGO	Virgo	LIGO	Virgo	
2015	3 months	40 – 60	–	40 – 80	–	0.0004 – 3
2016–17	6 months	60 – 75	20 – 40	80 – 120	20 – 60	0.006 – 20
2017–18	9 months	75 – 90	40 – 50	120 – 170	60 – 85	0.04 – 100
2019+	(per year)	105	40 – 80	200	65 – 130	0.2 – 200
2022+ (India)	(per year)	105	80	200	130	0.4 – 400

arXiv:1304.0670 (based on Class. Quantum Grav. 27 (2010) 173001)

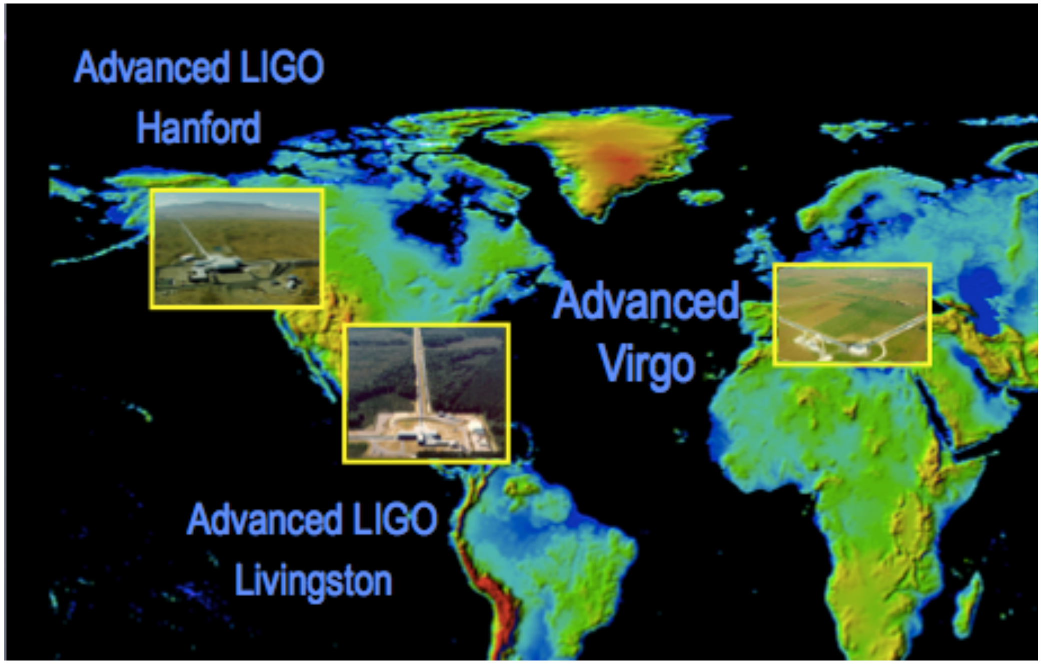

How many coalescences to expect? Gamma Ray Bursts

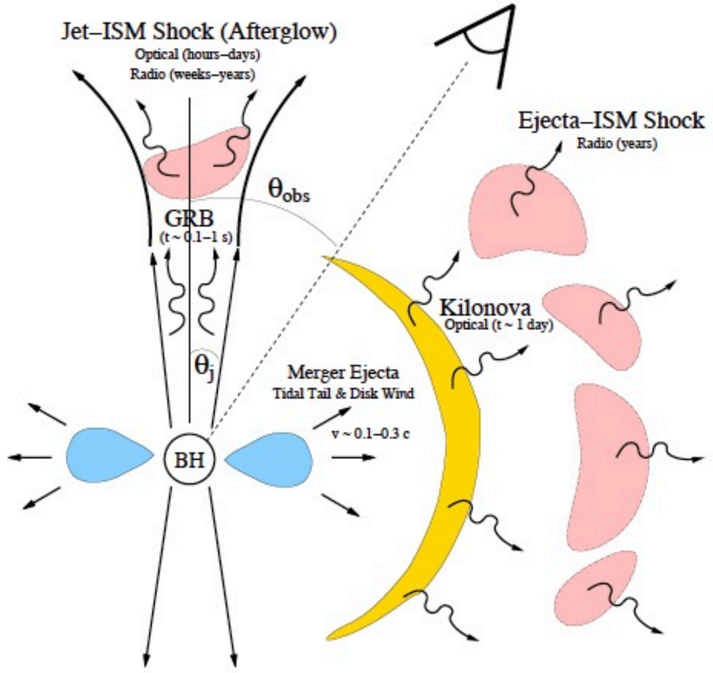

Figure 20:

Potential electromagnetic counterparts of compact object binary mergers as a function of the observer viewing angle (θ_{obs}). Rapid accretion of a centrifugally supported disk (blue) powers a collimated relativistic jet, which produces a short GRB. Due to relativistic beaming, the γ-ray emission is restricted to observers with $\theta_{obs} \lesssim \theta_j$. Afterglow emission results from the interaction of the jet with the circumburst medium (pink). Optical afterglow emission is detectable for observers with $\theta_{obs} \lesssim 2\theta_j$. Radio afterglow emission is observable from all viewing angles once the jet decelerates to mildly relativistic velocities on a timescale of months-years, and can also be produced on timescales of years from sub-relativistic ejecta. Short-lived isotropic optical/near-IR emission lasting a few days (kilonova; yellow) can also accompany the merger, powered by the radioactive decay of r-process elements synthesized in the ejecta. From Metzger & Berger (2012).

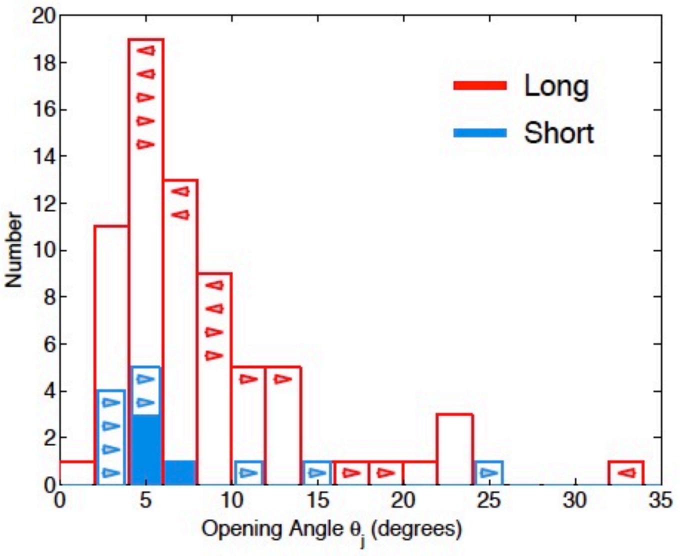

Figure 18:

Distributions of jet opening angles for short (blue) and long (red) GRBs, based on breaks in their afterglow emission. Arrows mark lower or upper limits on the opening angles. The observations are summarized in §8.4. From Fong et al. (2013) and references therein.

If beaming factor is ~ 70 (θ ~10°), [??]
source rate is ~1/Mpc^3/Myr,
similar to inferred from DNS in the galaxy (!).

DOI: 10.1146/annurev-astro-081913-035926
arXiv:1311.2603

The GW Detector Network~2020

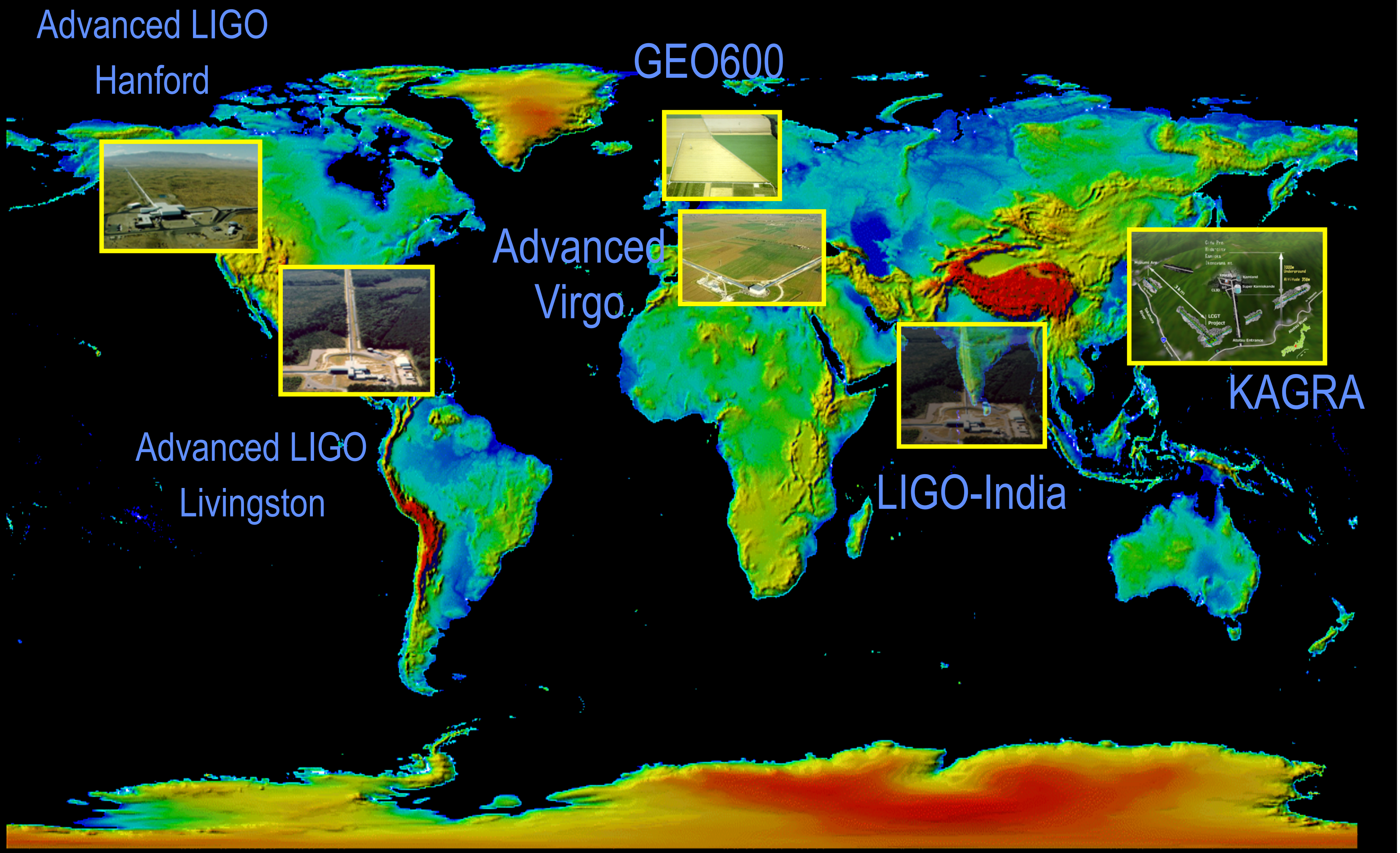

More detectors = better localization

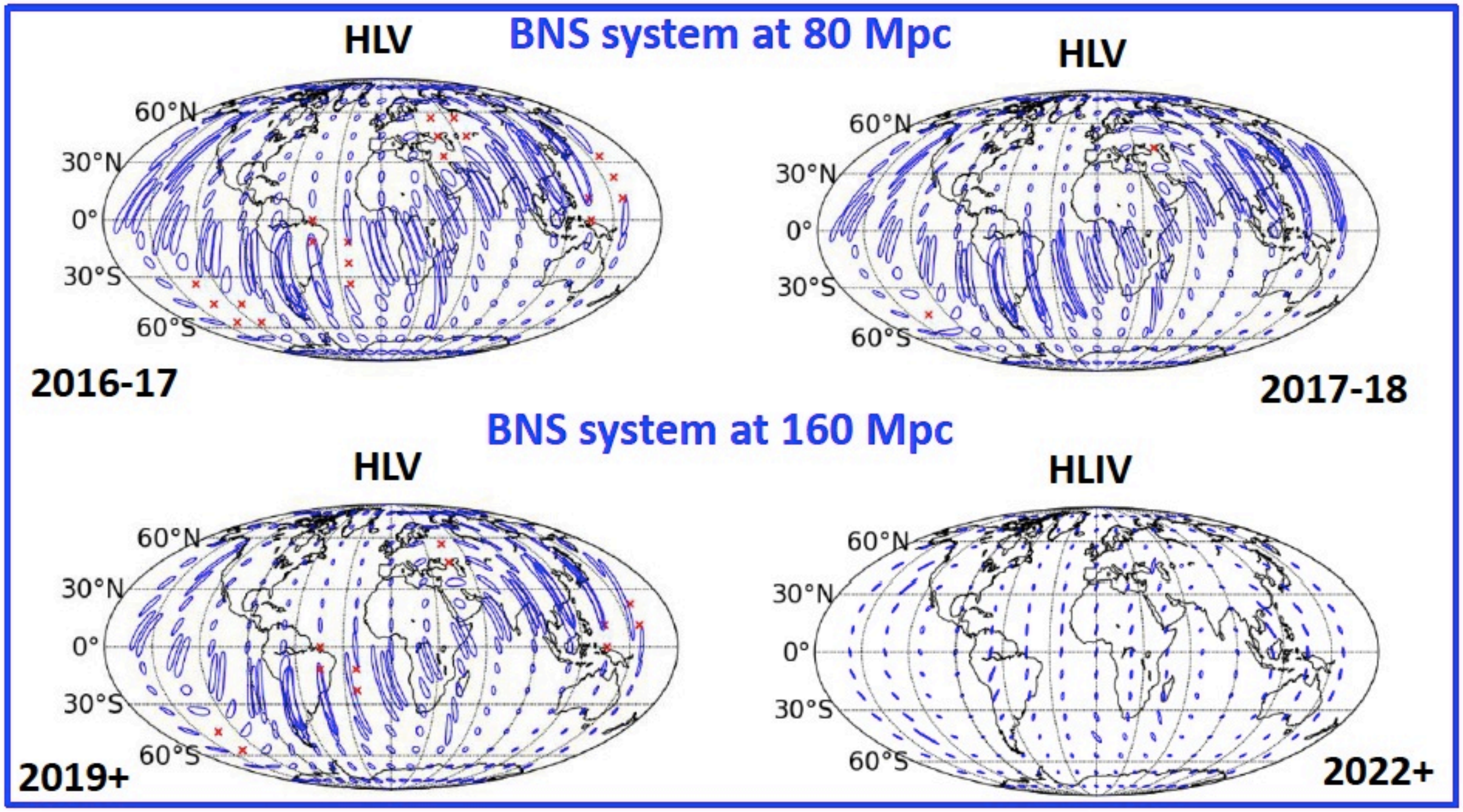

Position uncertainties with areas of **tens to hundreds of sq. degrees**

⬭ → 90% confidence localization areas

X → signal not confidently detected

Multi-messenger astronomy with Advanced GW Detectors

- After the first four published GW events, LSC and Virgo will promptly release public triggers to be followed up.
- To initiate the multi-messenger from the very beginning, LSC and Virgo opened a call to sign agreements for the identification of EM counterparts to GW triggers in Advanced detectors starting in 2015.
- We have signed more than 70 agreements with groups from 19 countries, with about 150 instruments covering the full EM spectrum, from radio to high-energy gamma-rays.

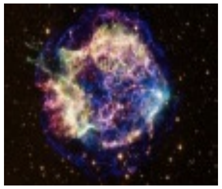

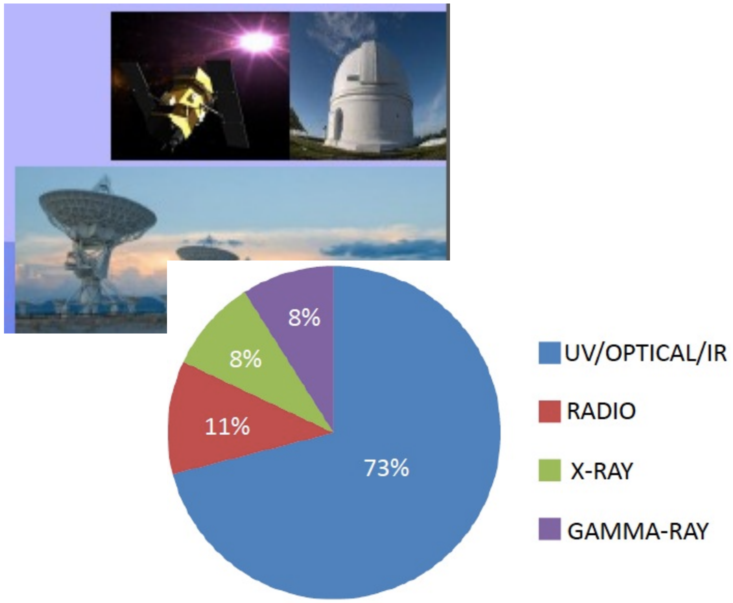

GW ground-based detectors: the future (perspective session)

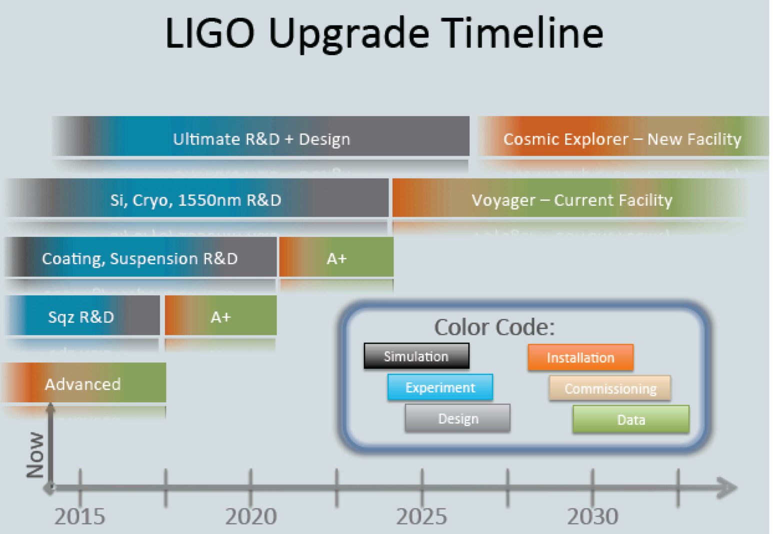

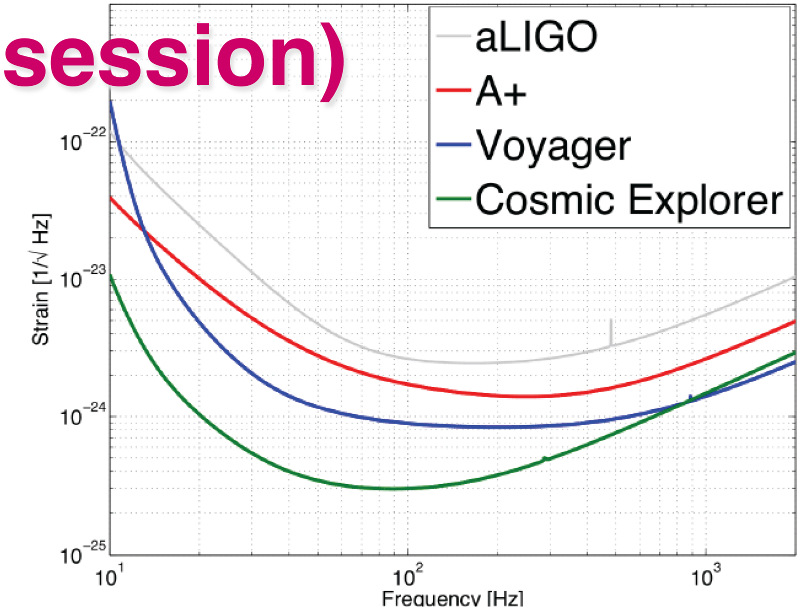

https://dcc.ligo.org/LIGO-T1400316/public

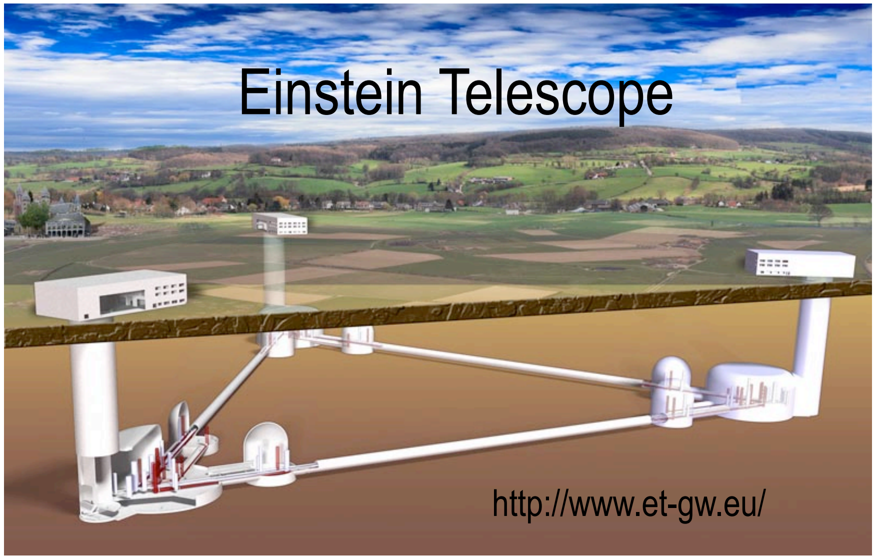

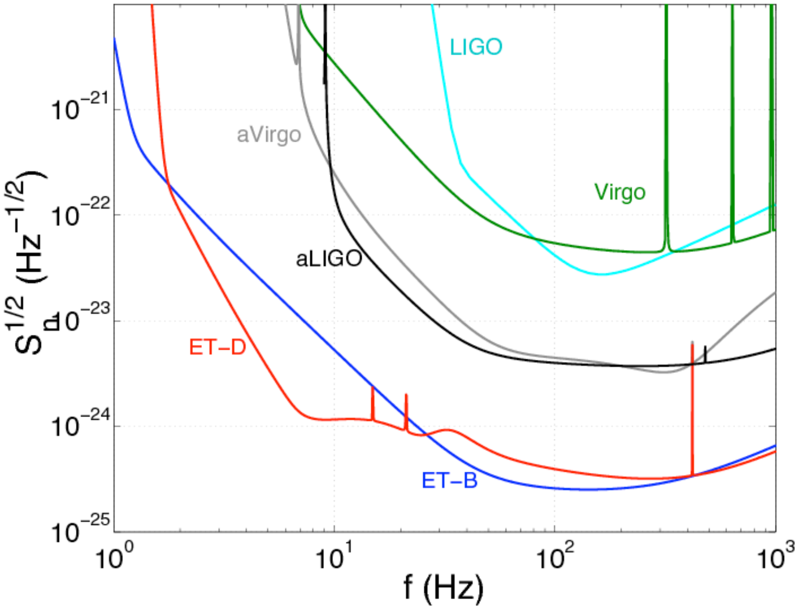

Gravitational waves are coming!